3-D SIMULATION OF INTERPENETRATING PHASE COMPOSITES USING FEM/EFGM

A DISSERTATION

Submitted in partial fulfillment of the requirements for the award of the degree of

MASTER OF TECHNOLOGY

in

MECHANICAL ENGINEERING

(With Specialization in CAD/CAM & Robotics)

By

PRAMOD KUMAR

DEPARTMENT OF MECHANICAL AND INDUSTRIAL ENGINEERING
INDIAN INSTITUTE OF TECHNOLOGY ROORKEE
ROORKEE-247 667 (INDIA)

JUNE, 2013

INDIAN INSTITUTE OF TECHNOLOGY ROORKEE

ROORKEE

CANDIDATE'S DECLARATION

I hereby declare that the work carried out in this dissertation titled "**3-D SIMULATION OF INTERPENETRATING PHASE COMPOSITES BY FEM/EFGM**" is presented on behalf of partial fulfilment of the requirement for the award of the degree of **Master of Technology** with specialization in **CAD, CAM & Robotics** submitted to the department of **Mechanical & Industrial Engineering, Indian Institute of Technology Roorkee, India**, under the supervision and guidance of **Dr. B. K. Mishra**, Professor and **Dr. I. V. Singh**, Associate Professor MIED, IIT Roorkee, India.

I have not submitted the matter embodied in this report for the award of any other degree or diploma.

Date: 14.06.2013

Place: **Roorkee**

(PRAMOD KUMAR)

CERTIFICATION

This is to certify that the above statement made by the candidate is correct to the best of our knowledge and belief.

(Dr. B. K. Mishra)

Professor
MIED
IIT Roorkee, India

(Dr. I. V. Singh)

Associate Professor
MIED
IIT Roorkee, India

ACKNOWLEDGEMENT

Various persons at various stages and in varied ways have played a key role in enabling me to give a final shape to my M. Tech. Dissertation work. No matter how small or insignificant form their point of view was the help rendered but for me it meant a lot. I owe to each and every one of them my heartfelt and shall endeavour to record my feelings within the ambit of this page.

I am deeply indebted to my guides **Dr. B. K. Mishra**, Professor and **Dr. I. V. Singh**, Associate Professor in the department of **Mechanical & Industrial Engineering**, **Indian Institute of Technology**, **Roorkee**, whose help, stimulating suggestions, motivation and encouragement helped me in all the time to make my effort successful. I really owe a lot to all my friends and batch-mates, especially to Mr. Azher Jameel, Mr. Vivek Kumar Sharma, Mr. Himanshu Yadav who helped me directly or indirectly during the entire period of this work.. Finally, I would like to thank my parents and family members whose constant support and love throughout the work helped me realised the dissertation to complete.

Pramod

Date: 14.06.2013

Place: Roorkee

PRAMOD KUMAR

Enrl No.: 11538008

ABSTRACT

Interpenetrating Phase Composites (IPCs) are multiphase composites where each phases is interconnected three- dimensionally. The lighter, stiffer stronger and tougher material is called metal phase and the other as reinforcement. They have unique geometry which offers improved mechanical and physical properties. According to the occurrence of the of the interpenetration at different length scales, IPCs can be categorised as molecular, micro or meso composites. This project provides a modelling and simulation of alumina- copper based IPC. The computational used to model and simulate the IPC is based on Element Free Galerkin Method (EFGM) using MATLAB.

Owing to complexity in microstructure & randomness of IPCs, the modelling of these materials have not been effectively studied yet. Two models have been proposed by the author one in two - dimension and another one in three- dimension. They are Unit- cell model which is based on the geometry of the sub-cell. A sub-cell is a collection of randomly generated quarter circle placed in the corner of a square in two- dimension and randomly generated cuboids placed in the corners of a cube in three- dimension. Many sub-cells are arranged together making a unit-cell. Degree of penetration is introduced which controls the geometry of the models between interpenetrating and particulate. Other parameters such as volume fraction, interpenetrating geometry have been incorporated into the model.

In this thesis two types of analysis is carried out on both the models. The elastic analysis includes finding out the equivalent elastic properties of the IPCs like Young's modulus, Shear modulus and Poisson's ratio. For this **effective medium approximation** technique has been used. In this technique the strain energy of the IPC is equated to that of the equivalent homogeneous medium. The elastic properties at certain volume fractions are found out and are validated with the experimental results and others available in the literatures. The elasto-plastic analysis for large values of starin is carried out to find the equivalent stress- strain curve of the IPC. The results are found to be within the limits and comparable to the results available in the literatures.

ABBREVIATIONS

$\mathbf{x}$	Sampling point coordinates (x,y,z)
$\mathbf{x}_I$	Node coordinates (x,y,z)
$\mathbf{u}$	Displacement field
$u^h(\mathbf{x})$	MLS approximation function for function u
$\mathbf{p}(\mathbf{x})$	Complete basis function
$\mathbf{a}(\mathbf{x})$	Vector of unknown coefficients
k'	Degree of the polynomial basis
m	Number of terms in the basis
$L(\mathbf{x})$	Weighted least square sum
u_I	Nodal parameter associated with node I
$w(\mathbf{x}-\mathbf{x}_I)$	Weight function having compact support associated with node I
$\psi_I(\mathbf{x})$	Shape function
$\psi_{I,\mathbf{x}}(\mathbf{x})$	Derivative of shape function with respect to spatial co-ordinates
$d_{\max}$	Scaling parameter which defines size of the domain of influence
$w_{,x}$	Derivative of weight function with respect to x
$w_{,y}$	Derivative of weight function with respect to y
$w_{,z}$	Derivative of weight function with respect to z
$\varphi_I(\mathbf{x})$	Level set function
$\varphi_{I,\mathbf{x}}(\mathbf{x})$	Derivative of level set function with respect to spatial co-ordinates
σ	Stress vector
$\mathbf{b}$	Body force vector
Ω	Domain
$\mathbf{n}$	Unit normal to the domain Ω

Γ_t	Traction boundary
Γ_u	Displacement boundary
$\delta \mathbf{W}_u$	Term to enforce the essential boundary conditions
$\mathbf{q}$	Vector of displacement boundary conditions
E	Modulus of elasticity
$N_{I(x)}$	Lagrange interploant
λ	Lagrange multiplier
ε	Strain tensor
$\mathbf{K}_{IJ}$	Global stiffness matrix
$\mathbf{B}_I$	Shape function matrix
$\mathbf{G}_{IK}$	Displacement matrix
ν	Poisson's ratio
$\mathbf{f}$	Force vector
G	Shear modulus
U	Strain energy density
$H(\mathbf{x})$	Heaviside function
$\mathbf{x}$	Sampling point coordinates
$\mathbf{x}_I$	Node coordinates
σ_y	Yield stress
σ_u	Ultimate stress
V_f	Volume fraction of a phase
$\overline{V}$	Volume

CHAPTER 1

INTRODUCTION

1.1 COMPOSITE MATERIAL

Composite materials are the materials of modern era. The composites for the desired purposes are made by mixing two or more different materials on a macroscopic scale. The mechanical & physical properties of the resultant material are better than those of the constituent materials. The one of constituent materials whose mechanical properties is stiffer and stronger is said to be reinforcement and other as matrix phase. The reinforcement phase is usually discontinuous. The matrix phase behaves as cementing to the reinforcement phase and usually continuous.

The mechanical properties, geometry and phase distribution of the constituent materials have bearing on the composite materials' mechanical properties. The volume fraction which is ratio of the reinforcement to the matrix phase is one of the most important parameter that governs the overall properties of the composite. The homogeneity of the composite material system is determined by the distribution of the reinforcement. The shape and direction of reinforcement affects the anisotropy of the system. Out of constituents' materials the matrix is the main load bearing which provides protection for the sensitive reinforcement.

There is wide application of composite materials. Aerospace, aircraft, marine, automotive, sport, energy, and biomedical industries have used composites in various ways. The advantageous properties of composites like high stiffness, high strength, and low density make way to be used in both military and civilian aircraft widely. For prosthetic devices and artificial limb parts various composites are used. In aerospace structures the light weight and extremely stiff graphite composites are used. In Sporting goods such as tennis rackets, golf clubs, fishing poles, skis and bicycles the composites got wider applications.

1.2 INTERPENETRATING PHASE COMPOSITES (IPC)

The matrix phase of conventional composites is usually continuous. It behaves as a binder to the reinforcement phase which is discontinuous. The binding ability, the thermal capability to the reinforcing phase and low cost are the basis on which matrix phase is chosen. Nowadays, new variety of composites is being prepared with both the phases being continuous. They have a network of interpenetration of reinforcement impregnated in molten metal. Therefore, they are known as **INTERPENETRATING PHASE COMPOSITES (IPCS)**

IPC may be defined as multiphase materials. Where all phases are interconnected three dimensionally throughout the structure. Interpenetrating Phase Composites may have two or more than two phases which are interconnected in a way that it will be difficult to distinguish between reinforcing and matrix phases based on states of continuity and isolation. The previous problem of matrix dominating influence on the composites is removed by the dual continuity of the phases. The reinforcement's unique geometry offers superior mechanical properties of the resultant composites. Owing to complete continuity each constituent phases may contribute its properties to the macroscopic of the composites' properties. Many fascinating properties of all the constituent phases are retained in the resultant composite raising the hope of developing materials having actual composite behaviour. According to interpenetration at various length scales, IPC can be divided into molecular, micro or meso varieties.

Therefore , Interpenetrating Phase Composites offer the hope of actual composite, where two usually incompatible properties of pure materials may co- exist in a composite.

Figure 1.1: 3D microstructure of an IPC

Figure 1.2: 2D cross-section of a 2 phase IPC

1.2.1 Applications and Advantages of IPCs

The near-net IPC's shape capability, low production cost and good tribological performance offers the IPC's suitability for the applications like automotive disc brake rotors, internal combustion (IC) engine piston crowns, connecting rods, cylinder liners, robot arms, turbine compressors, callipers, etc. Further, the enhanced properties at high temperatures offer them suitability for aerospace usage. IPC has good bio- medical usage, too.

Varioius researchers have found that IPC has enhanced mechanical and physical properties than other composites. The main advantage of the IPC is the interconnectivity of both the phases that makes it possible for both the phases to impart their advantageous properties to the composite in a better manner. The matrix phase still dominates the thermo-mechanical behaviour while inter-metallic phase improves toughness by crack bridging mechanism. Newer manufacturing methods have made IPC of lower thermal expansion, good compression, higher stiffness, & bending strength.

The ceramic phase gives it high strength and high modulus while metallic phase gives low density, good toughness. Moreover, presence of a continuous structure will provide higher strength and enhanced high temperature properties & thermal stability. The IPC are known for their improved wear resistance because of their complex and random microstructure, with an added advantage of isotropic nature. Interpenetrating Phase Composites are environment friendly as they can be easily recycled.

1.3 OBJECTIVE

The fracture mechanics of these materials have not been sufficiently studied so far because of complex and random behaviour of IPC. Agarwal *et al* (2012) have tried to simulate using two dimensional model which is the simplest one and compared the model with the available models so far. The main objective of the project is to simulate near net shape of the composites that is three dimensional structures and to compare with the available models including the two dimensional one proposed by Agarwal *et al* (2012,2013). Therefore, the aim of the dissertation is to develop versatile computational algorithm that will model and simulate the different dynamics of these materials so that we will be able to understand, design and predict newer composites with shorter lead-time without much expense.

The main problems, which will be tackled in this project, are:

1. To study of the interpenetrating microstructure and its effects on the macro scale.
    a. Three dimensional modelling and approximation of the effective medium in the IPC (EMA).
    b. To validate the model with the available literatures.
    c. Results of different IPCs (obtained by different combination of the phases) are compared with particulate composites of similar nature.
2. To develop a micro-model (local model), which will approximate the randomness in the geometry of the IPC.
3. To study of parameters influencing the strength of an IPC
    a. To calculate of strength of IPC with the appropriate use of EMA (global model) and local model.
    b. To validate the model developed with results available in literature and experimentation.
4. To find the effective Mechanical properties of the IPC.

CHAPTER 2

LITERATURE REVIEW

2.1 ELEMENT FREE GALERKIN METHOD

A number of meshfree methods has been developed to analyse problems encountered by FEM/EFGM) (Belytschko *et al.*, 1994; Lu *et al.*, 1994) is the most frequently used method for analysing solid mechanics problems. They used EFGM for arbitrary shape elasticity problems as well as simple heat conduction problems, the rate of convergence in this method is higher than the other method. They applied this method to analyse quasi static crack growth problems.

Belytscko *et al.* (1995a,b; 1996a,b) used EFGM in static and dynamic crack growth problems. Their results by the EFGM method were very close to analytical approach. The problem of remeshing was removed. However, the computational time increased by 50%.

Krongauz (1996) in his doctoral thesis proposed a method for incorporating the discontinuous derivatives in EFGM. His method was applicable for one and two-dimensional problems only..

Dolbow and Belytschko (1999) proposed some modification in numerical integration of Galerkin weak form for meshless method. A new structure of integration cells was suggested which lessened the quadrature error.

Belytschko *et al.*, (1999) suggested a technique for modelling discontinuities. Jump function was used to model material discontinuity and for near crack tip enrichment Westergard's solution was used. They proposed vector level set to model crack.

Pant *et al.*, (2010) developed methods for modelling material discontinuities with the use of level set functions. They suggested a signed distance function to enrich those nodes which are close to the interface and provide a discontinuous strain function.

2.2 INTERPENETRATING PHASE COMPOSITE (IPCs)

2.2.1 Introduction

Liu and Koster (1995) were probably the earliest researchers who proposed the manufacturing technique of Interpenetrating Phase Composites (IPCs). They made Al_2O_3- Al metal matrix(MM) composite by impregnating silica perform with molten Al.

Zhou *et al.* (1998) suggested self-propagating high temperature synthesis reaction technique to make porous matrix phase of Al_2O_3-TiC. They infiltrated this with pure aluminium (Al) in Nitrogen pressurized furnace at 750°C. Some volatile agents were used to increase the porosity of the SHS products.

Horvitz *et al.* (2002) did some modification in the SHS reaction to incorporate wider range of materials by introducing Reactive Thermal explosion and hot pressing technique. Thus, after initial heating due to an increased exothermic release of energy the reaction became self sufficient.

Yu and Xiao-lu (2006) made IPC using a vacuum assisted low negative pressure moulding process. In this process, pure aluminium foams were infiltrated with different polymers. Quasi-static compression tests were done at room temperature. The composites show improved compressive behaviour and improved energy absorption capacity compared with the pure aluminium foam. Experimental modulus data is well within H-S bounds,too.

Han *et al.* (2006) propose Al_2O_3- Ti_3Al IPC by dry milling of the constituent powder by high energy discuss milling device followed by pressure less sintering. XRD results suggested reduction in particle size and enhanced homogeneity. Few other characteristics are increased hardness, decreased porosity etc. Due to debonding of alumina and aluminide interface and crack bridging of ductile Ti_3Al phase the fracture toughness improved substantilly.

Jhaver and Tippur (2009) made IPC using pressure less infiltration technique on syntactic aluminium foam. A number of uni-axial compression test was carried out on syntactic foam & IPC foam and then results were compared. They used unit cell in the form of Kelvin cell (tetrakaidecahedron) with using triangular aluminium ligaments and rest of the space is filled by syntactic foam. FEM analysis was done in ABAQUS and was found to be matching with experimental results.

Marchi *et al.* (2003) made Alumina–Al IPC with 3-D periodic structure. They used Fused Deposition Method and Direct Write Method to produce sintered Al_2O_3 tower in a graphite block. Al rods are then placed on the top of graphite to produce random isotropic IPC. Thermal expansions were measured using push rod dialometer. Aluminium bars carry increased proportion of transverse tensile stress.

Vecchia *et al.* (2003) made Al_2O_3-Al IPC using Reactive Metal Penetration (RMP) method. They studied various microscopic and mechanical characteristics of the IPC using different experimental techniques. They found a strong variation in both the microstructure and the orientation of the metallic phase channels in different cross sections of the composite.

They extensively studied and reasoned the different microstructures at different cross sections of the IPC. They also studied the mechanical behavior such as thermal expansion, bending compression and tensile properties and fracture mechanics of the IPC.

Kouzeli and Dunand (2003) observed the results of the elasto-plastic behaviour of reinforcement Aluminium composite. The comparative higher stiffness owe to interconnectivity is moderate (10% avg Al composite). For dominating interconnection of reinforcement, the ratio of stiffness needs to be enhanced. Also, increase in volume fraction of stiffer reinforcement would increase the compressive & stiffness flow stresses of MM-IPC.

2.2.2 Modelling and Simulation

Wegner and Gibson (2000) used 3-D printing method to produce stainless steel – bronze IPC. They used non-linear FEM model according to unit cell model having periodic boundary conditions. Dimensions were based on volume fractions of respective phases. The elastic modulus estimated by Finite Element analyses lie within the narrow band of Hashin-Shtrikman bounds, confirming the suitability of the model. They concluded that there is a purpose to examine the influence of contact region between sintered particles on flow properties.

Agrawal *et al.* (2003) calculated the thermal residual stresses in 02 IPC (Al/Al_2O_3 & Cu/Al_2O_3). They found that metallic phase contain tensile stresses and the ceramic phase has compressive stresses. These stresses generate due to difference in volume fraction, melting point, stiffness in the two phases. This creates residual stresses when cooled during manufacturing. FEM modeling is done in ANSYS to find numerical results.

Tilbrook *et al.* (2005) modelled alumina epoxy IPC based on three techniques which included Iso stress – Iso Strain Approximation Model, Effective Medium Approximation (EMA) and Unit Cell Model. They also used Impulse Excitation Technique (IET) to experimentally calculate the elastic moduli of IPC.

Feng *et al.* (2003) suggested an efficient method to predict elastic moduli. They used two-step procedure to measure the moduli: The effective elastic modulus of cubic cell was estimated using FEM or simple iso- stress and iso- strain model for the parallel and series combination of unit cell.

Tohgo *et al.* (2006) developed a model for two phases IPC by introducing a matricity into the constituent equations of particulate composites. The matricity can be thought of as a representation of the true volume fractions. They considered the IPC as two particulate

composite with respective matrix and reinforcement interchanged. By this method, they calculated the moduli of elasticity and poisson's ratio of different phases. Thus, they applied successfully to FGM using FEM techniques.

Poniznik *et al.* (2008) suggested a FEM which is based on approximation of IPC structure. A cubical IPC is divided into numbers of cuboids (voxel). The number of voxels selected based on the volume fraction of the phase. Also care must be taken to select voxels so that each is connected by at least an edge of another voxel. No voxel should be left out. Then FEM modelling of this cube will give us the effective mechanical properties of the IPC.

2.2.3 Strength and Fracture analysis

Prielipp *et al.* (1995) observed the strength & fracture toughness of Al_2O_3-Aluminium IPC. They found that Al infiltration increases the fracture strength.

Zhou *et al.* (1999) studied the IPC using XRD (X-Ray diffraction). They observed plastic deformation at crack tip thus leading to uneven and torturous fracture surface. They noted strong interfacial bond strength.

Pezzotti and Sbaizero (2001) experimentally substantiated relations between microscopic stress fields and macroscopic crack bridging. They used fluorescence microprobe spectroscopy technique to measure the microscopic residual and bridging stress fields produced during cooling of Al_2O_3-Al IPC. A crack was introduced externally and its propagation was studied. R curve was plotted which was compared with theoretical R-curve. They found a relation between R-curve and bridging stresses, which could explain the fracture characteristics of these complex materials.

Bin *et al.* (2002) used squeeze casting to intrude the molten metal into the highly porous SHS products. This method gave an increased strength regardless of increased porosity.

Agrawal and Sun (2004) studied fracture in metal-ceramic composites. They compared two IPCs (Al/Al_2O_3 & Cu/Al_2O_3) and one particulate composite (Al/SiC). They found that fracture toughness is proportional to the ductile particle size up to a critical limit and beyond that thermal residual stress weakens the interface. The FEM modelling is done based on global/local approach. The globally effective properties were calculated with the help of EMA. Then near the crack tip, a local region is taken into account and thus microstructure properties are accounted for.

Etter *et al.* (2004) measured the fracture & strength of graphite–Al IPC made by investment casting method. Flexural test using four point bending test was done. Fracture

toughness test was performed using modified SEVNB with notch tip radii of 30 μm. Thermal fatigue testing was done between 30°C to 300°C.

Mayer and Papakyriacou (2006) observed the fatigue cracks generally initiate at porosity by interface failure. Infiltration improves tensile and bending strength but cyclic properties are less affected.

Moon *et al.* (2008) evaluated crack tip stress fields on a micro scale. They used Single edge V notch bend(SEVNB) test with notch diameter of 25 μm and measured the stress distributions using Fluorescence spectroscope. Also crack growth was observed under four point bend fixture loading (that promoted subcritical crack growth). They noted that the crack moves to avoid reinforcement phase in low volume fraction of reinforcement. In high volume fraction of reinforcement crack becomes discontinuous and reinitiates elsewhere. They also proposed a FEM model in which they used the actual geometry near the crack region.

Dukhan *et al.* (2010) AFPC by immersing an aluminium foam matrix with an unfilled polypropylene homo polymer. They measured the flexural properties of this material for 5 different specimens; these were found to be close to lower bounds the reason of which is yet to be found out. However, there is a an increase by one and half in elastic moduli.

2.3 PROGRESSIVE DAMAGE MODELLING

Fao *et al.* (1993) studied the microscopic images of SiC interfaces. They characterised the reason behind strong and weak interfaces. The faceted interface which form a chemical bond have strong interface. The inter-metallic compounds found lodged at the interface makes the interface weak.

Ravichandran, 1994 proposed an iterative method to predict the deformation behaviour of IPC using an unit cell model. Prielipp *et al* (1994) described the mechanical properties of Al/Al_2O_3 composite in terms of volume fraction and ligament diameter. They proposed a mathematical model based on the two parameters to calculate fracture strength of the composite.

Kapoor and Vecchio (1995) examined the deformation behaviour and failure mechanism in 6061 Al MMC. Both tensile and compressive behaviour depend on T4 and T6 condition and relative strength of particle and matrix. In compression the particle merely acts as obstacles to the flow of matrix, while in tension the particles assist in the flow.

Doel and Bowen (1995) carried out uniaxial tensile testing on MMC. Low particle size increases the 0.2% proof stress and ultimate strength and high particle size increases the

same. Ductility is reduced. Damage is initiated by void nucleation. they also found that small particle reinforcement damage less easily and are more ductile.

Kashyap *et al.,* (1999) postulated that the strengthening of MMC is associated with high dislocation density and its work hardening effect. The role of work hardening parameters in strengthening of MMC was investigated.

Fleming and Temis (2002) analysed the behaviour of AlSiC MMC under cyclic loading using models based on strain cyclic plasticity and strain accumulated damage. They mathematically modelled elasto-plastic deformation process in MMC.

Pyo and Lee (2010) proposed a damage model considering imperfect interface to predict effective elasto-plastic behaviour of MMC. They used modified Eshelby tensor with weakened interfaces. They used a progressive damage model to numerically simulate the multilevel interfacial damage model.

Reddy and Zitour (2010) determined the mechanical properties of different particle reinforced MMC. The yield strength, ultimate strength and ductility depends not only on the reinforcing agent but the type of matrix alloy also.

Hertele *et al.,*(2010) gave a method to combine different types of stress-strain models to form a generic stress-strain model to represent the behaviour of any type of composite. They used Ramberg-Osgood model as it is most versatile and valid over large strains.

Agarwal *et al.,* (2012) presented two models namely Unit-Cell and Self-Consistent Model the elastic properties of IPCs to find out elastics properties of them. They duly incorporated all influencing parameters such as volume fraction, degree of penetration & random geometry. These models were analysed by a meshless method known as EFGM. They found that the unit-cell model is easy to implement and less time consuming.

Agarwal *et al.,* (2013) used Ramberg-Osgood material model to model the elasto-plastic behaviour of the composites. They proposed a progressive damage model based on the treatment of the interface. They found that the ultimate strength and the yield strength of the IPC depened mainly on the properties, volume fraction and interpenetration of the constituent phases. Their result were found to be in good agreement with the experimental ones.

2.4 RESEARCH GAP

Due to complexity and randomness in microstructure, the mechanics of these materials have not been sufficiently studied so far. The basic objective of this dissertation is to model and simulate the failure phenomenon in IPC to understand, design and predict newer composites with shorter lead-time without much expense since the experimentation is difficult, and time consuming, therefore there is need to develop a versatile computational algorithm, which will simulate the different dynamics of these materials.

CHAPTER 3

ELEMENT FREE GALERKIN METHOD

3.1 INTRODUCTION

The element free Galerkin method is quite different from FEM as no element and element connectivity data is needed but only a set of nodes over the given domain along with boundary description is required to construct the approximation function (shown in **Fig. 3.1**).

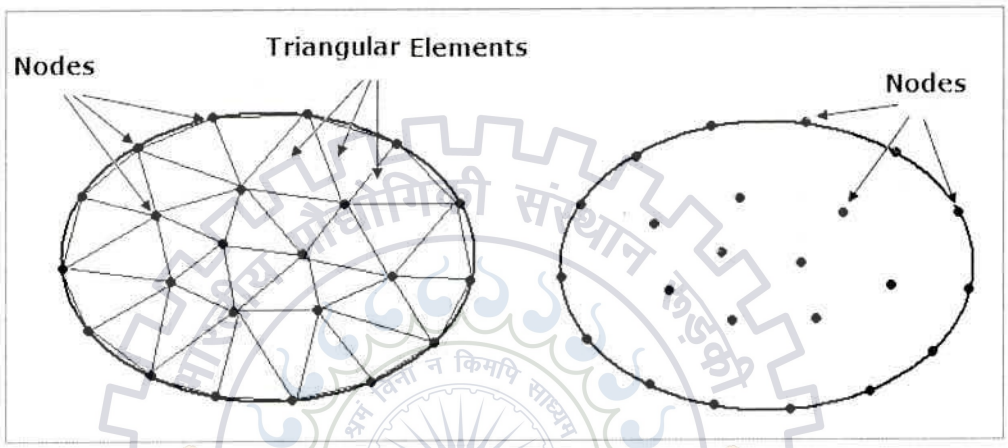

Fig. 3.1: Domain representation in FEM and EFGM

In EFGM, both trial and test functions are constructed from the same space using moving least square (MLS) approximants.

The MLS approximants consists of three components:

- A compact support weight function associated with each node,
- A polynomial basis function and
- A set of coefficients that depends on node position.

4.2 WEIGHT FUNCTION

The support of the weight function defines the nodal domain of influence, over which a particular node contributes to the approximation. The overlap of the node's domain of influence defines the nodal connectivity as shown in **Fig.3.2**. Circular or rectangular domain of influence is used for 2-D problems but in case of 3-D, circular domain of influence becomes spherical and rectangular domain of influence becomes cuboidal. One useful property of MLS approximation is that their continuity is governed by the continuity of

weight functions. Therefore, a highly continuous approximation function can be generated by an appropriate choice of weight function.

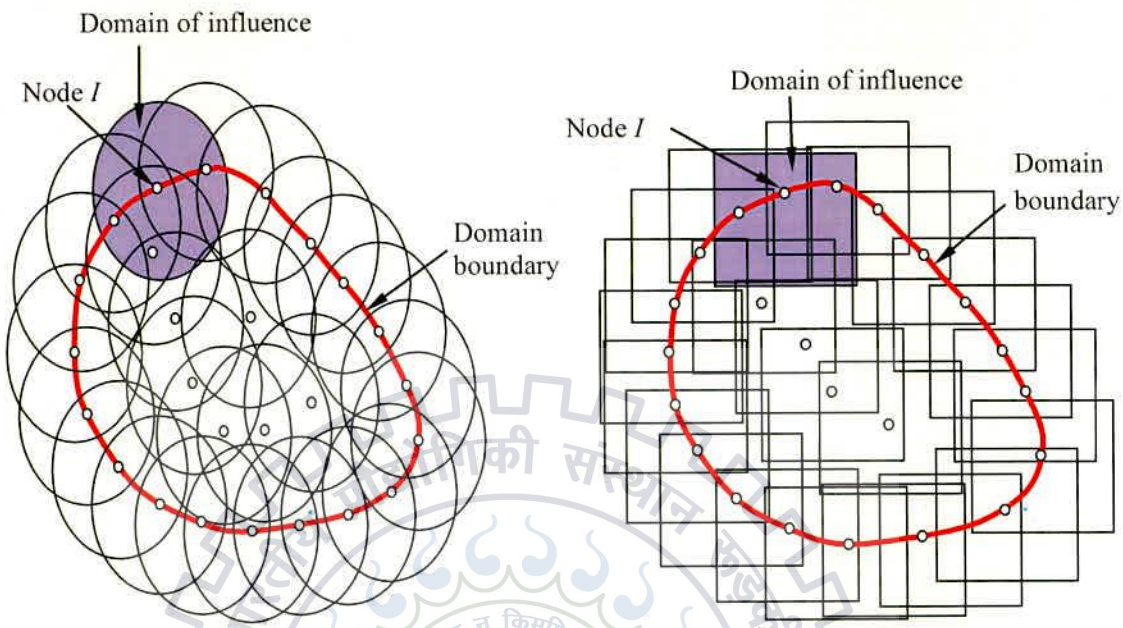

Fig. 3.2: A computational model of rectangular and circular domain of influence

For the numerical simulation, different weight functions are used which illustrated here.

Cubic spline:

$$w(r)=\begin{cases}\dfrac{2}{3}-4r^2+4r^3, & r\le\dfrac{1}{2}\\[2ex] \dfrac{4}{3}-4r+4r^3-\dfrac{4}{3}r^3, & \dfrac{1}{2}<r\le 1\\[2ex] 0, & r>1\end{cases} \tag{3.1}$$

Quartic spline:

$$w(r)=\begin{cases}1-6r^2+8r^3-3r^4, & r\le 1\\ 0, & r>1\end{cases} \tag{3.2}$$

Simple exponential:

$$w(r)=\begin{cases}e^{-\left(\frac{r}{c}\right)^{2k}}, & r\le 1\\ 0, & r>1\end{cases} \tag{3.3}$$

Guassinan exponential:

$$w(r)=\begin{cases}\dfrac{e^{-\left(\frac{r}{c}\right)^{2k}}-e^{-\left(\frac{1}{c}\right)^{2k}}}{1-e^{-\left(\frac{1}{c}\right)^{2k}}}, & r\le 1\\ 0, & r>1\end{cases} \tag{3.4}$$

where, c is the dilation parameter and k is the number is terms in polynomial basis function. Normalized radius for spherical domain of influence is given by

$$r=\frac{\|x_I-x\|}{d_I} \tag{3.5}$$

where, d_I is the support domain of node I. For cuboidal domain of influence, normalized radius is

$$r=\left(\frac{|x_I-x|}{d_I^x}\right)\left(\frac{|y_I-y|}{d_I^y}\right)\left(\frac{|z_I-z|}{d_I^z}\right) \tag{3.6}$$

where, d_I^x, d_I^y, d_I^z is the support domain of node I in the x, y, z directions. Cubic and quartic weight function for eight nodded 10 unit length bar are plotted with $d_{\max}=1.25$ given in **Fig. 3.3**

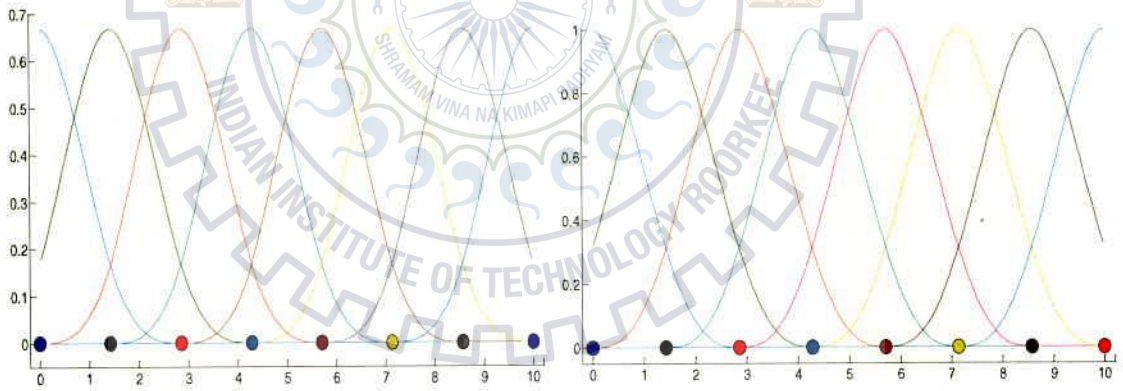

Fig. 3.3: Cubic and quartic spline weight functions 1-D

Cubic and quartic weight function for single node of plate of 2×2 unit area are plotted with $d_{\max}=1.25$ given in **Fig. 3.4**

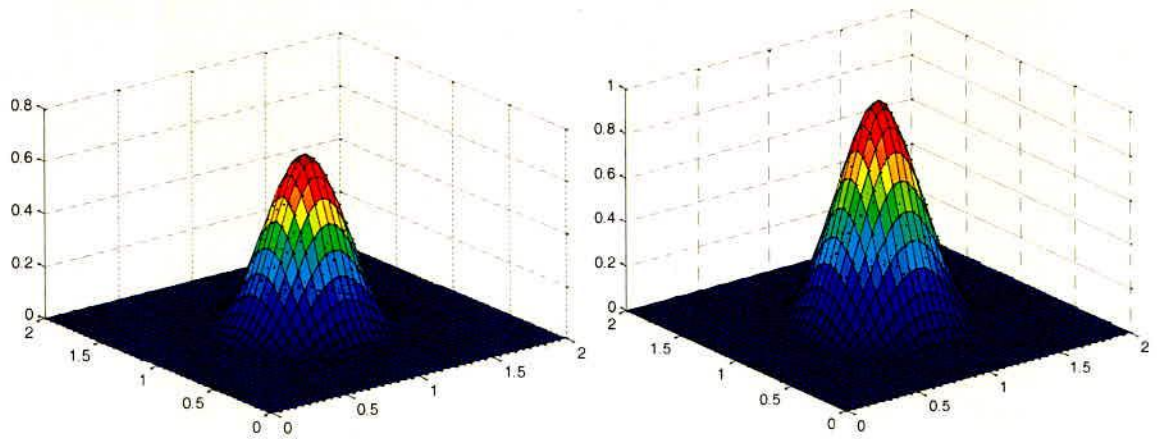

Fig. 3.4: Cubic and quartic spline weight functions 2-D

3.3 MOVING LEAST SQUARE (MLS) APPROXIMATIONS

The MLS approximation has two major features that make it popular:

- The approximated field function is continuous and smooth in the entire problem domain.
- It is capable of producing an approximation with the desired order of consistency.

In EFGM, the approximation of $u(x)$ at any point $x = \Re^N$ in the domain $\Omega \subseteq \Re^N$, where $N = 1, \text{or} 2, \text{or} 3$ is denoted as $u^h(x)$, given by MLS approximation

$$u^h(\mathbf{x}) = \sum_{j=1}^{k} p_j(\mathbf{x}) a_j(\mathbf{x}) \equiv \mathbf{p}^T(\mathbf{x})\mathbf{a}(\mathbf{x}) \tag{3.7}$$

where, $\mathbf{p}^T(\mathbf{x}) = [p_1(\mathbf{x}), p_2(\mathbf{x}), \cdots, p_k(\mathbf{x})]$ is a basis of order k and $p_j(\mathbf{x})$ is a vector of complete basis functions (usually polynomial). For three dimensions ($N = 3$) and $\mathbf{x}^T = [x \quad y \quad z]$.

$$\mathbf{p}^T(\mathbf{x}) = [1 \;\; x \;\; y \;\; z] \qquad \text{(linear basis)} \tag{3.8}$$

$$\mathbf{p}^T(\mathbf{x}) = [1 \;\; x \;\; y \;\; z \;\; xy \;\; yz \;\; zx \;\; x^2 \;\; y^2 \;\; z^2] \qquad \text{(quadratic basis)} \tag{3.9}$$

$$\mathbf{p}^T(\mathbf{x}) = [1, \; x, \; y, \; z, \; xy, \; yz, \; zx, \; \ldots \; x^{k'}, \; y^{k'}, \; z^{k'}] \qquad (\text{k}^{\text{th}} \text{ order basis}) \tag{3.10}$$

and $\mathbf{a}^T(\mathbf{x}) = [a_1(\mathbf{x}), \; a_2(\mathbf{x}), \; a_3(\mathbf{x}), \; \ldots, a_k(\mathbf{x})]$ is a vector of unknown coefficients $a_j(\mathbf{x})$ which depends on position i.e. $\mathbf{x}$.

The unknown coefficients $\mathbf{a}(\mathbf{x})$ are obtained by minimizing a weighted least square sum of the difference between local approximation, $u^h(\mathbf{x})$ and field function nodal parameter

u_I. The weighted least square sum denoted by $L(\mathbf{x})$ can be written in following quadratic form:

$$L(\mathbf{x}) = \sum_{I=1}^{n} w(\mathbf{x}-\mathbf{x}_I)[u^h(\mathbf{x}) - u_I]^2 \tag{3.11}$$

On substitution of Eq. (4.7) into Eq. (4.11)

$$L(\mathbf{x}) = \sum_{I=1}^{n} w(\mathbf{x}-\mathbf{x}_I)[\mathbf{p}^T(\mathbf{x}_I)\mathbf{a}(\mathbf{x}) - u_I]^2 \tag{3.12}$$

where, u_I is the nodal parameter associated with node I at $\mathbf{x} = \mathbf{x}_I$ but $u^h(\mathbf{x} = \mathbf{x}_I)$ is not the nodal values of because $u^h(\mathbf{x})$ as an approximant not an interplant as shown in **Fig. 3.5** and n is the number of nodes for which $w(\mathbf{x}-\mathbf{x}_I) > 0$.

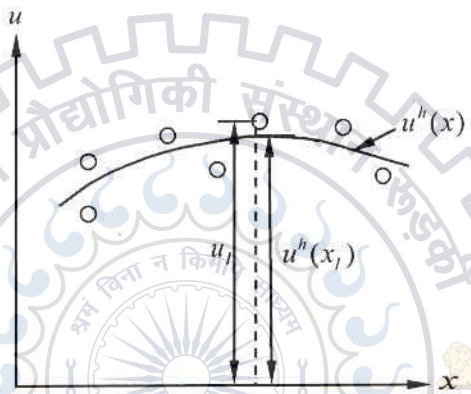

Fig. 3.5: Difference between u_I and $u^h(\mathbf{x})$

The minimization of L i.e. $\dfrac{\partial L}{\partial \mathbf{a}} = 0$, leads to following expression:

$$\begin{aligned}
&\frac{\partial L}{\partial a_1} = 0 \Rightarrow \sum_{I=1}^{n} w(\mathbf{x}-\mathbf{x}_I)\,2\,p_1(\mathbf{x}_I)[\mathbf{p}^T(\mathbf{x}_I)\mathbf{a}(\mathbf{x}) - u_I] = 0 \\
&\frac{\partial L}{\partial a_2} = 0 \Rightarrow \sum_{I=1}^{n} w(\mathbf{x}-\mathbf{x}_I)\,2\,p_2(\mathbf{x}_I)[\mathbf{p}^T(\mathbf{x}_I)\mathbf{a}(\mathbf{x}) - u_I] = 0 \\
&\quad\vdots \qquad\qquad\qquad\qquad\qquad\qquad\qquad\qquad = \vdots \\
&\frac{\partial L}{\partial a_k} = 0 \Rightarrow \sum_{I=1}^{n} w(\mathbf{x}-\mathbf{x}_I)\,2\,p_k(\mathbf{x}_I)[\mathbf{p}^T(\mathbf{x}_I)\mathbf{a}(\mathbf{x}) - u_I] = 0
\end{aligned} \tag{3.13}$$

In vector notation

$$\sum_{I=1}^{n} w(\mathbf{x}-\mathbf{x}_I)\,2\,\mathbf{p}(\mathbf{x}_I)\left[\mathbf{p}^T(\mathbf{x}_I)\,\mathbf{a}(\mathbf{x}) - u_I\right] = 0 \tag{3.14}$$

$$2\sum_{I=1}^{n} w(\mathbf{x}-\mathbf{x}_I)\,\mathbf{p}(\mathbf{x}_I)\,\mathbf{p}^T(\mathbf{x}_I)\,\mathbf{a}(\mathbf{x}) - w(\mathbf{x}-\mathbf{x}_I)\,\mathbf{p}(\mathbf{x}_I)\,u_I = 0 \tag{3.15}$$

After arranging Eq. (3.15)

$$\mathbf{a}(\mathbf{x}) = \left[\sum_{I=1}^{n} w(\mathbf{x}-\mathbf{x}_I)\mathbf{p}(\mathbf{x}_I)\mathbf{p}^T(\mathbf{x}_I)\right]^{-1} \sum_{I=1}^{n} w(\mathbf{x}-\mathbf{x}_I)\mathbf{p}(\mathbf{x}_I)u_I \tag{3.16}$$

Substituting $\mathbf{a}(\mathbf{x})$ into Eq. (3.7), the MLS approximation is obtained as:

$$u^h(\mathbf{x}) \equiv \mathbf{p}^T(\mathbf{x})\left[\sum_{I=1}^{n} w(\mathbf{x}-\mathbf{x}_I)\mathbf{p}(\mathbf{x}_I)\mathbf{p}^T(\mathbf{x}_I)\right]^{-1} \sum_{I=1}^{n} w(\mathbf{x}-\mathbf{x}_I)\mathbf{p}(\mathbf{x}_I)u_I \tag{3.17}$$

This can be written as

$$u^h(\mathbf{x}) \equiv \underbrace{\mathbf{p}^T(\mathbf{x})}_{1\times k}\ \underbrace{\mathbf{A}^{-1}(\mathbf{x})}_{k\times k}\ \underbrace{\mathbf{B}(\mathbf{x})}_{k\times n}\ \underbrace{\mathbf{u}}_{n\times 1} \tag{3.18}$$

and $$\mathbf{a}(\mathbf{x}) = \mathbf{A}^{-1}(\mathbf{x})\mathbf{B}(\mathbf{x})\mathbf{u} \tag{3.19}$$

where, $\mathbf{A}(\mathbf{x})$ and $\mathbf{B}(\mathbf{x})$ are given as:

$$\mathbf{A}(\mathbf{x}) = \sum_{i=1}^{n} w(\mathbf{x}-\mathbf{x}_I)\mathbf{p}(\mathbf{x}_I)\mathbf{p}^T(\mathbf{x}_I) = w(\mathbf{x}-\mathbf{x}_1)\begin{bmatrix} 1 & \mathbf{x}_1 \\ \mathbf{x}_1 & \mathbf{x}_1^{\,2} \end{bmatrix} + \cdots + w(\mathbf{x}-\mathbf{x}_n)\begin{bmatrix} 1 & \mathbf{x}_n \\ \mathbf{x}_n & \mathbf{x}_n^{\,2} \end{bmatrix} \tag{3.20}$$

$$\mathbf{B}(\mathbf{x}) = [w(\mathbf{x}-\mathbf{x}_1)\mathrm{p}(\mathbf{x}_1), \cdots, w(\mathbf{x}-\mathbf{x}_n)\mathrm{p}(\mathbf{x}_n)] = \left\{ w(\mathbf{x}-\mathbf{x}_1)\begin{bmatrix} 1 \\ \mathbf{x}_1 \end{bmatrix}, \ldots, w(\mathbf{x}-\mathbf{x}_n)\begin{bmatrix} 1 \\ \mathbf{x}_n \end{bmatrix} \right\} \tag{3.21}$$

Meshfree approximation can be given as

$$u^h(\mathbf{x}) = \sum_{I=1}^{n} \psi_I(\mathbf{x})u_I = \boldsymbol{\psi}(\mathbf{x})\mathbf{u} \tag{3.22}$$

where,

$$\boldsymbol{\psi}(\mathbf{x}) = [\psi_1(\mathbf{x})\ \psi_2(\mathbf{x})\ \psi_3(\mathbf{x})\ \cdots\ \psi_n(\mathbf{x})] \tag{3.23}$$

$$\mathbf{u}^T = [u_1\ \ u_2\ \ u_3\ \cdots\ u_n] \tag{3.24}$$

By comparing Eqs. (3.18, 3.22), the MLS shape functions are defined as:

$$\boldsymbol{\psi}(\mathbf{x}) = \underbrace{\mathbf{p}^T(\mathbf{x})\mathbf{A}^{-1}(\mathbf{x})\mathbf{B}(\mathbf{x})}_{1\times n} \tag{3.25}$$

The MLS shape function for node I $\psi_I(\mathbf{x})$ is defined as:

$$\psi_I(\mathbf{x}) = \underbrace{\mathbf{p}^T\mathbf{A}^{-1}w(\mathbf{x}-\mathbf{x}_I)\mathbf{p}(\mathbf{x}_I)}_{1\times 1} = \mathbf{p}^T\mathbf{A}^{-1}\mathbf{B}_I \tag{3.26}$$

The derivatives of MLS shape function are computed as:

$$\psi_{I,\mathbf{x}}(\mathbf{x}) = (\mathbf{p}^T\mathbf{A}^{-1}\mathbf{B}_I)_{,\mathbf{x}} = \mathbf{p}^T{}_{,\mathbf{x}}\,\mathbf{A}^{-1}\mathbf{B}_I + \mathbf{p}^T(\mathbf{A}^{-1})_{,\mathbf{x}}\mathbf{B}_I + \mathbf{p}^T\mathbf{A}^{-1}\mathbf{B}_{I,\mathbf{x}} \tag{3.27}$$

where,

$$\mathbf{B}_{I,\mathbf{x}}(\mathbf{x}) = \frac{dw}{d\mathbf{x}}(\mathbf{x}-\mathbf{x}_I)\mathbf{p}(\mathbf{x}_I) \tag{3.28}$$

and $\mathbf{A}^{-1}{}_{,x}$ is computed by

$$\mathbf{A}^{-1}{}_{,x} = -\mathbf{A}^{-1}\mathbf{A}_{,x}\mathbf{A}^{-1} \tag{3.29}$$

where,

$$\mathbf{A}_{,x} = \sum_{I=1}^{n} \frac{dw}{d\mathbf{x}}(\mathbf{x} - \mathbf{x}_I)\mathbf{p}(\mathbf{x}_I)\mathbf{p}^T(\mathbf{x}_I) \tag{3.30}$$

Here, comma designates a partial derivative with respect to the indicated spatial variable. MLS shape functions and their derivatives are plotted for linear and quadratic polynomial basis having cubic spline weight function for eight nodded 10 unit length bar with d_{max} = 1.25 shown in **Fig. 4.6-4.7.**

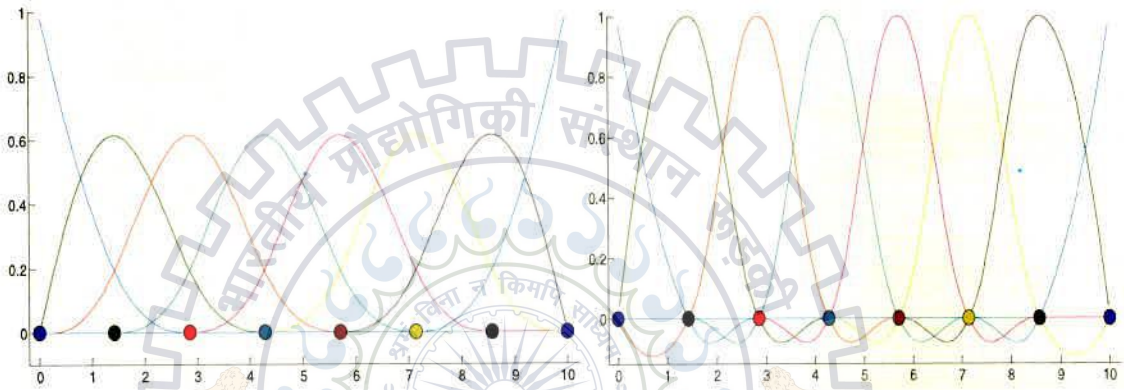

Fig. 3.6: MLS shape functions with linear and quadratic polynomial

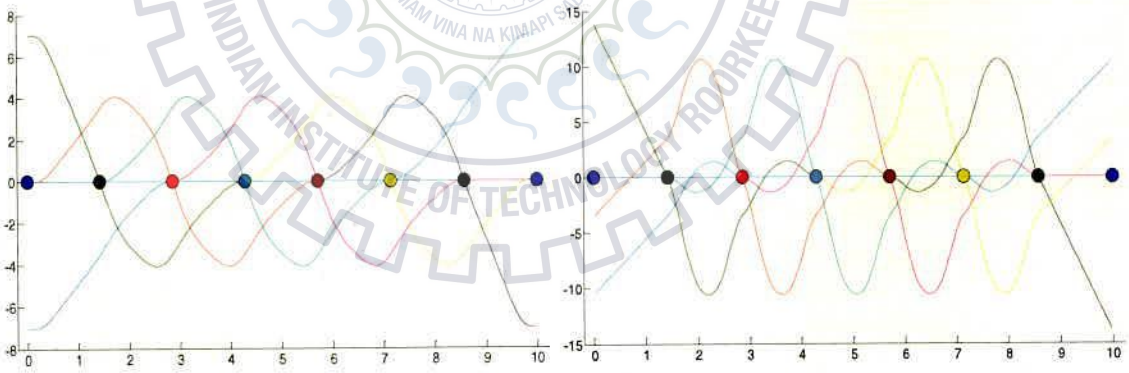

Fig. 3.7: Derivative of MLS shape functions having linear and quadratic polynomial basis

For linear basis quartic spline weight function and shape function are shown in **Fig. 3.8** for 2-D while the derivatives of shape function are plotted in **Fig. 3.9**, d_{max} = 1.25 is used for this case.

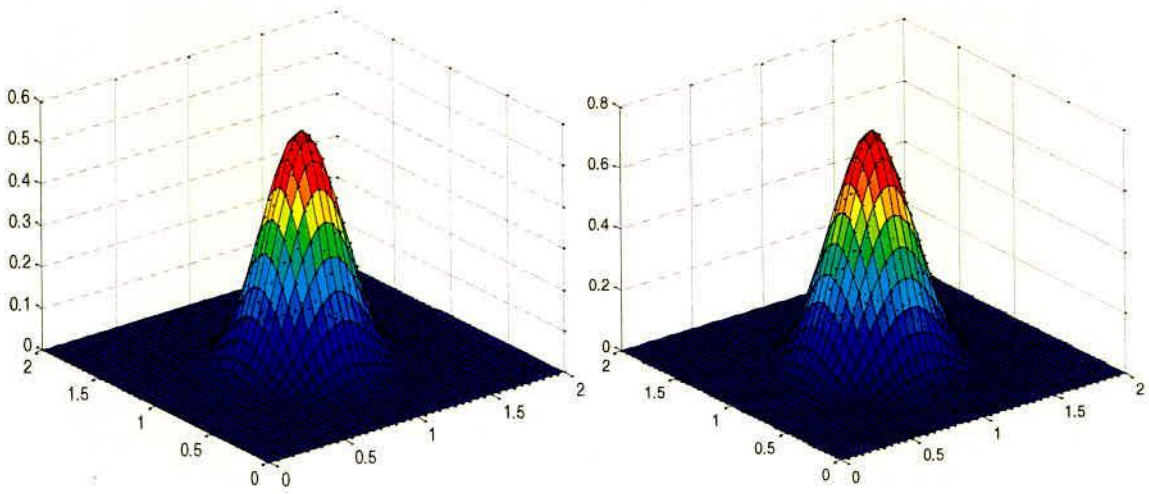

Fig. 3.8: Cubic and quartic spline MLS shape functions

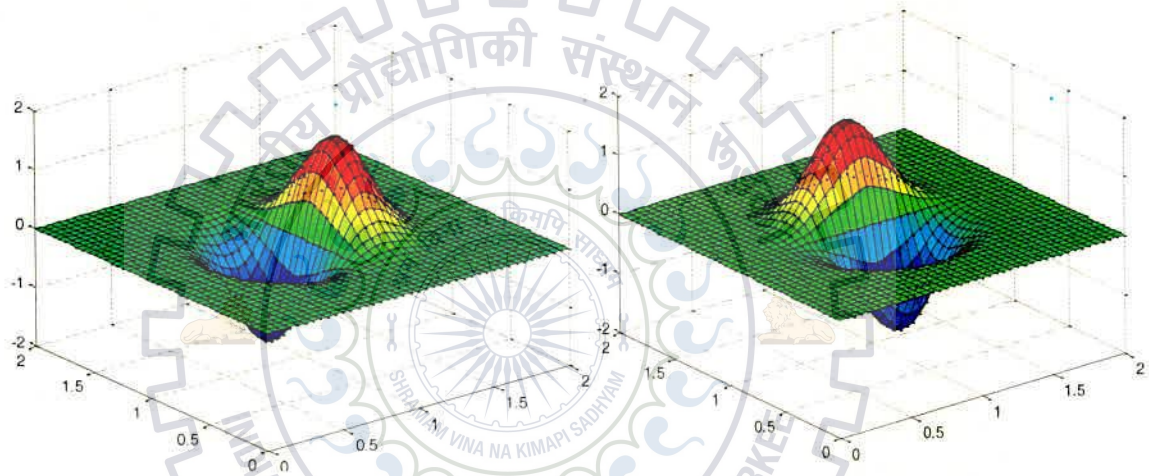

Fig. 3.9: Derivative of cubic spline MLS shape functions w.r.t. x and y

3.4 ENFORCEMENT OF ESSENTIAL BOUNDARY CONDITIONS

The proper imposition of essential boundary condition is quite difficult in EFGM since MLS approximation does not satisfy the Kronecker delta function property i.e. $\psi_I(x_J) \neq \delta_{IJ}$. Many numerical techniques have been proposed to enforce the essential boundary conditions in EFGM.

- Lagrange multiplier approach is quite accurate but its imposition loses the positive definite and bandedness properties of the system matrix. It generates more number of unknown in the solution.
- In coupling with FEM, EFGM domain is necklaced by FEM domain, and then essential boundary conditions are applied in the same manner as in FEM.

- ❖ Penalty approach is easy for the enforcement of the essential boundary conditions, and it gives discrete equations in simple form similar to FEM. Although, system matrix obtained by this method is positive and posses bandedness property but improper selection of penalty parameter may lead to wrong results.

In this work, Lagrange multiplier approach is employed along with point collocation scheme.

3.5 EFGM FORMULATION BASED ON MINIMUM POTENTIAL ENERGY APPROACH

In EFGM, an approximate solution for a node I having n number of nodes under its domain of influence, is given as

$$u_I^h(\mathbf{x}) = \psi_1(\mathbf{x})u_1 + \psi_2(\mathbf{x})u_2 + \cdots + \psi_n(\mathbf{x})u_n \tag{3.31}$$

$$v_I^h(\mathbf{x}) = \psi_1(\mathbf{x})v_1 + \psi_2(\mathbf{x})v_2 + \cdots + \psi_n(\mathbf{x})v_n \tag{3.32}$$

$$w_I^h(\mathbf{x}) = \psi_1(\mathbf{x})w_1 + \psi_2(\mathbf{x})w_2 + \cdots + \psi_n(\mathbf{x})w_n \tag{3.33}$$

where, $\psi_1, \cdots, \psi_n$ are the partition of unity MLS shape functions, $u_1, v_1, w_1, \cdots, u_n, v_n, w_n$ are the unknown displacements at the nodes $(1, \cdots, n)$ in the Cartesian coordinate system. The above equation can be written in matrix form as

$$\begin{Bmatrix} u \\ v \\ w \end{Bmatrix} = \begin{bmatrix} \psi_1(\mathbf{x}) & 0 & 0 & \cdots & \psi_n(\mathbf{x}) & 0 & 0 \\ 0 & \psi_1(\mathbf{x}) & 0 & \cdots & 0 & \psi_n(\mathbf{x}) & 0 \\ 0 & 0 & \psi_1(\mathbf{x}) & \cdots & 0 & 0 & \psi_n(\mathbf{x}) \end{bmatrix} \begin{Bmatrix} u_1 \\ v_1 \\ w_1 \\ \vdots \\ u_n \\ v_n \\ w_n \end{Bmatrix} \tag{3.34}$$

In vector form

$$\underbrace{\mathbf{u}}_{3\times 1} = \underbrace{[\boldsymbol{\psi}]}_{3\times n}\ \underbrace{\{\mathbf{U}\}}_{n\times 1} = \{\mathbf{U}\}^T [\boldsymbol{\psi}]^T \tag{3.35}$$

The strain at any point can be obtained as

$$\underbrace{\boldsymbol{\varepsilon}}_{6\times 1} = \underbrace{[\mathbf{B}_{std}]}_{6\times n}\underbrace{\{\mathbf{U}\}}_{n\times 1} \tag{3.35}$$

where,

$$[\mathbf{B}_{std}] = \begin{bmatrix} \frac{\partial \psi_1(\mathbf{x})}{\partial x} & 0 & 0 & \cdots & \frac{\partial \psi_n(\mathbf{x})}{\partial x} & 0 & 0 \\ 0 & \frac{\partial \psi_1(\mathbf{x})}{\partial y} & 0 & \cdots & 0 & \frac{\partial \psi_n(\mathbf{x})}{\partial y} & 0 \\ 0 & 0 & \frac{\partial \psi_1(\mathbf{x})}{\partial z} & \cdots & 0 & 0 & \frac{\partial \psi_n(\mathbf{x})}{\partial z} \\ 0 & \frac{\partial \psi_1(\mathbf{x})}{\partial z} & \frac{\partial \psi_1(\mathbf{x})}{\partial y} & \cdots & 0 & \frac{\partial \psi_n(\mathbf{x})}{\partial z} & \frac{\partial \psi_n(\mathbf{x})}{\partial y} \\ \frac{\partial \psi_1(\mathbf{x})}{\partial z} & 0 & \frac{\partial \psi_1(\mathbf{x})}{\partial x} & \cdots & \frac{\partial \psi_n(\mathbf{x})}{\partial z} & 0 & \frac{\partial \psi_n(\mathbf{x})}{\partial x} \\ \frac{\partial \psi_1(\mathbf{x})}{\partial y} & \frac{\partial \psi_1(\mathbf{x})}{\partial x} & 0 & \cdots & \frac{\partial \psi_n(\mathbf{x})}{\partial y} & \frac{\partial \psi_n(\mathbf{x})}{\partial x} & 0 \end{bmatrix}, \quad \{\mathbf{U}\} = \begin{Bmatrix} u_1 \\ v_1 \\ w_1 \\ \vdots \\ u_n \\ v_n \\ w_n \end{Bmatrix}, \quad \boldsymbol{\varepsilon} = \begin{Bmatrix} \varepsilon_x \\ \varepsilon_y \\ \varepsilon_z \\ \gamma_{yz} \\ \gamma_{zx} \\ \gamma_{xy} \end{Bmatrix} \tag{3.36}$$

Total potential energy of the system is defined as

$$\Pi = \frac{1}{2}\int_{\Omega}(\varepsilon_x\sigma_x + \varepsilon_y\sigma_y + \varepsilon_z\sigma_z + \gamma_{yz}\sigma_{yz} + \gamma_{zx}\sigma_{zx} + \gamma_{xy}\sigma_{xy})d\Omega - \int_{\Omega}(uf_x + vf_y + wf_z)d\Omega - \int_{\Gamma_t}(ut_x + vt_y + wt_z)d\Gamma_t \tag{3.37}$$

Eq. (3.37) can be written in matrix form as

$$\Pi = \frac{1}{2}\int_{\Omega}\begin{bmatrix}\varepsilon_x & \varepsilon_y & \varepsilon_z & \gamma_{yz} & \gamma_{zx} & \gamma_{xy}\end{bmatrix}\begin{Bmatrix}\sigma_x \\ \sigma_y \\ \sigma_z \\ \sigma_{yz} \\ \sigma_{zx} \\ \sigma_{xy}\end{Bmatrix}d\Omega - \int_{\Omega}\begin{bmatrix}u & v & w\end{bmatrix}\begin{Bmatrix}f_x \\ f_y \\ f_z\end{Bmatrix}d\Omega - \int_{\Gamma_t}\begin{bmatrix}u & v & w\end{bmatrix}\begin{Bmatrix}t_x \\ t_y \\ t_z\end{Bmatrix}d\Gamma \tag{3.38}$$

where, f_x, f_y, f_z are the body forces per unit volume and t_x, t_y, t_z are the surface tractions at node I in x, y, z-directions respectively. In concise form, it is given by

$$\Pi = \frac{1}{2}\int_{\Omega}\boldsymbol{\varepsilon}^T\boldsymbol{\sigma}\,d\Omega - \int_{\Omega}\mathbf{u}^T\mathbf{f}\,d\Omega - \int_{\Gamma_t}\mathbf{u}^T\mathbf{t}\,d\Gamma_t \tag{3.39}$$

The essential boundary condition (**Fig. 4.10**) are defined as

$$\mathbf{u} = \bar{\mathbf{u}} \qquad \text{on} \qquad \Gamma_u \tag{3.40}$$

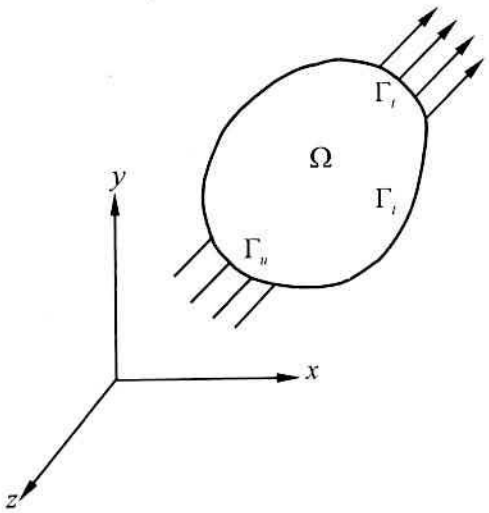

Fig. 3.10: Domain with applied boundary conditions

Here, the superposed bar denotes prescribed values. In this paper, Lagrange multiplier method has been considered to enforce the essential boundary conditions. The Lagrange multiplier λ is expressed as

$$\lambda(\mathbf{x}) = N_I(s)\boldsymbol{\lambda}_I, \qquad \mathbf{x} \in u \tag{3.41}$$

$$\delta\lambda(\mathbf{x}) = N_I(s)\delta\boldsymbol{\lambda}_I, \qquad \mathbf{x} \in u \tag{3.42}$$

where, $N_I(s)$ is Lagrange interpolants and s is the arc length along the boundary for node I. Incorporating the essential boundary condition.

$$\tilde{\Pi} = \Pi - \int_{\Gamma_u} \lambda^T (\mathbf{u} - \bar{\mathbf{u}})\, d\Gamma_u \tag{3.43}$$

Hence, Eqs. (3.39, 3.43) yields

$$\tilde{\Pi} = \frac{1}{2}\int_{\Omega} \boldsymbol{\varepsilon}^T \boldsymbol{\sigma}\, d\Omega - \int_{\Omega} \mathbf{u}^T \mathbf{f}\, d\Omega - \int_{\Gamma_t} \mathbf{u}^T \mathbf{t}\, d\Gamma_t - \int_{\Gamma_u} \lambda^T (\mathbf{u} - \bar{\mathbf{u}})\, d\Gamma_u \tag{3.44}$$

Minimizing the potential energy expression with respect to unknowns u_1, v_1, w_1 ..... u_n, v_n, w_n, λ leads to

$$\int_{\Omega} \delta\boldsymbol{\varepsilon}^T \boldsymbol{\sigma}\, d\Omega - \int_{\Omega} \delta\mathbf{u}^T \mathbf{f}\, d\Omega - \int_{\Gamma_t} \delta\mathbf{u}^T \mathbf{t}\, d\Gamma_t - \int_{\Gamma_u} \delta\lambda^T (\mathbf{u} - \bar{\mathbf{u}})\, d\Gamma_u - \int_{\Gamma_u} \delta\mathbf{u}^T \lambda\, d\Gamma_u = 0 \tag{3.45}$$

Using following constitutive relations

$$\boldsymbol{\sigma} = \mathbf{D}\boldsymbol{\varepsilon} \tag{3.46}$$

By substituting Eqs. (3.35, 3.46) into Eq. (3.45) yields

$$\delta \mathbf{U}^T \underbrace{\int_{\Omega} \mathbf{B}_{std}^T \mathbf{D} \mathbf{B}_{std}\, d\Omega}_{\mathbf{K}} \mathbf{U} - \delta \mathbf{U}^T \underbrace{\left(\int_{\Omega} \boldsymbol{\psi}^T \mathbf{f}\, d\Omega + \int_{\Gamma_t} \boldsymbol{\psi}^T \mathbf{t}\, d\Gamma_t \right)}_{\mathbf{f}} - \delta \lambda^T \underbrace{\int_{\Gamma_u} -\mathbf{N}^T \boldsymbol{\psi} d\Gamma_u}_{\mathbf{G}^T} \mathbf{U}$$

$$+ \underbrace{\delta \lambda^T \int_{\Gamma_u} -\mathbf{N}^T d\Gamma_u}_{\mathbf{q}} - \underbrace{\delta \mathbf{U}^T \int_{\Gamma_u} -\boldsymbol{\psi}^T \mathbf{N} d\Gamma_u}_{\mathbf{G}} \lambda = 0 \tag{3.47}$$

It can be written as

$$\delta \mathbf{U}^T (\mathbf{K}\mathbf{U} - \mathbf{f} + \mathbf{G}\lambda) + \delta \lambda^T (\mathbf{G}^T \mathbf{U} - \mathbf{q}) = 0 \tag{3.48}$$

In matrix form

$$\begin{bmatrix} \mathbf{K} & \mathbf{G} \\ \mathbf{G}^T & 0 \end{bmatrix} \begin{Bmatrix} \mathbf{U} \\ \lambda \end{Bmatrix} = \begin{Bmatrix} \mathbf{f} \\ \mathbf{q} \end{Bmatrix} \tag{3.49}$$

where,

$$\mathbf{K} = \int_{\Omega} \mathbf{B}_{std}^T \mathbf{D} \mathbf{B}_{std}\, d\Omega \tag{3.50}$$

$$\mathbf{G} = -\int_{\Gamma_u} \boldsymbol{\psi} \mathbf{N} d\Gamma_u \tag{3.51}$$

$$\mathbf{f} = \{\mathbf{F}_b\} + \{\mathbf{F}_t\} \tag{3.52}$$

$$\mathbf{F}_b = \int_{\Omega} \boldsymbol{\psi}^T \begin{Bmatrix} f_x \\ f_y \\ f_z \end{Bmatrix} d\Omega \tag{3.53}$$

$$\mathbf{F}_t = \int_{\Gamma_t} \boldsymbol{\psi}^T \begin{Bmatrix} t_x \\ t_y \\ t_z \end{Bmatrix} d\Gamma_t \tag{3.54}$$

$$\mathbf{q} = -\int_{\Gamma_u} \mathbf{N} \bar{\mathbf{u}}\, d\Gamma_u \tag{3.55}$$

where, D is the constitutive matrix for a three dimensional linear elastic material, which can be written as

$$D = \frac{E}{(1+\nu)\times(1-2\nu)} \begin{bmatrix} (1-\nu) & \nu & \nu & 0 & 0 & 0 \\ \nu & (1-\nu) & \nu & 0 & 0 & 0 \\ \nu & \nu & (1-\nu) & 0 & 0 & 0 \\ 0 & 0 & 0 & (0.5-\nu) & 0 & 0 \\ 0 & 0 & 0 & 0 & (0.5-\nu) & 0 \\ 0 & 0 & 0 & 0 & 0 & (0.5-\nu) \end{bmatrix} \tag{3.56}$$

E is the Young's modulus and ν is the Poisson's ratio.

$$\mathbf{N} = \begin{bmatrix} N & 0 & 0 \\ 0 & N & 0 \\ 0 & 0 & N \end{bmatrix} \tag{3.57}$$

In this work, point collocation method has been used which assumes that the collocation points are coincident to nodes of displacement boundary whose degree of freedoms are restricted. Hence for 3-D case, **N** matrix becomes 3×3 an identity matrix.

3.6 NUMERICAL INTEGRATION

The computation of stiffness matrix ($\mathbf{K}$), displacement matrix ($\mathbf{G}$) and force vector ($\mathbf{f}$) requires an integration over the domain. Integrating the stiffness matrix and force vector requires a numerical integration scheme such as Gauss quadrature, which in turn, requires a subdivision of the domain.

There are two approaches available in literature for this purpose: first one is element quadrature in which the vertices of this background mesh are often used as the initial array of nodes for the EFGM model. However, it needs to create cells/elements inside the domain, and Guass points are generated inside these elements as shown in **Fig. 3.11(a)**. The black colour cross marks are the Guass points generated inside the elements. These Guass points are used for the numerical integration over the domain.

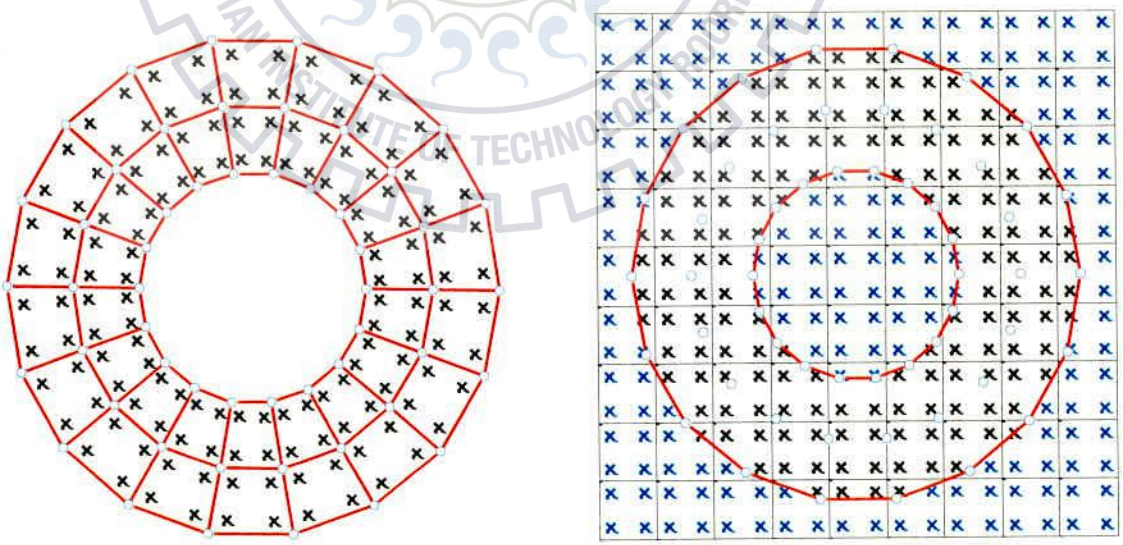

Fig. 3.11: (a) Element quadrature (b) Cell quadrature

The second integration technique, which is often called cell quadrature uses a background

grid of cells independent of the problem domain. During numerical at each integration point, it is necessary to find whether it lies inside the domain or not before integrating the Eqs. (3.50 - 3.54). This technique is not widely used as it does not yield good accuracy along curved and angled boundaries. **Fig. 3.11(b)** illustrates that only black colour cross marks are the Guass points which are used for integration as they lie inside the domain of interest. However, the blue colour cross marks are the Guass points which are generated in the background mesh but not used for integration hence this scheme becomes computationally more expensive than element quadrature.

3.7 DOMAIN OF INFLUENCE

The domain of influence or nodal support is an important aspect of meshfree methods; therefore its value must be chosen properly. The size of the support should be sufficiently large so that the stiffness matrix remains regular and well conditioned. But too large domains of influence lead to a great deal of computational expense in forming the approximations as well as in the assembly of stiffness matrix. The scaling parameter, $d_{\max}$ is typically taken as 1.25-3 for static analysis and 2 - 2.5 for dynamic analysis

CHAPTER 4

MECHANICS OF COMPOSITE MATERIALS

Traditional monolithic materials may be broadly categorised as metals, polymers & ceramics. Composites can be made by combining two or more materials from one or more of these categories.

4.1 GEOMETRY

The geometry of the composite material exhibits a defining role in the mechanical properties of composite materials. Based on the number of phases a material can be called single phase (monolithic), two phase, three phase or multi- phase material.

In **homogenous** material properties are same at every point. Homogeneity concept is associated with a scale or characteristic volume. Based on the scale parameter material can be homogenous or less homogenous. If the variability on a macroscopic scale is low the material is said to be quasi-homogenous. A material is known as heterogeneous if its properties vary from point to point at a particular scale. Depending on the scale parameter same material can be regarded as homogenous, quasi-homogenous, or heterogeneous.

Many material properties like stiffness, strength, thermal expansion, and permeability are associated with a direction. In isotropic material the properties are same in all directions. A material is known as an **anisotropic** when its properties at a point vary with direction or that depend on the orientation of reference axes. **Orthotropic** materials are the materials having at least three mutually perpendicular planes of symmetry. All these properties depend on the scale or characteristic volume, too.

4.2 MICROMECHNICS OF COMPOSITES

One of the main objectives of micromechanics is to obtain functional relationships for average elastic properties of the composite, such as stiffness in the form

$$C^* = f(C_f, C_m, V_f, S, A)$$

where,

C^* = average composite stiffness

C_f, C_m = fibre and matrix stiffness respectively

V_f = fibre volume fraction

S, A = geometric parameters describing the shape and array of the reinforcement respectively.

A lots of methods have been found to get the properties of the composite materials like

- Mechanics of Materials approach
- Numerical Techniques approach
- Self- Consistent field approach
- Variational Approach
- Semi- Empirical Approach
- Experimental Approach

The mechanics of materials approach is depended upon simple assumptions of either uniform strain or uniform stress in the constituents' material. The properties which are not sensitive to fibre shape and distribution such as Young's Modulus E_1 and major Poisson's ratio υ_{12} are predicted accurately by this approach.

Numerical Technique approaches like Finite difference, FEM, Periodic cell, or BEM give the best results. But these methods take more time and do not give closed form expressions.

Self-Consistent field approach is based on a simplified composite model is considered containing of a typical fibre confined by a cylindrical matrix phase. The properties constituents are similar to the average properties of the composite material.

Variational methods are based on energy principles and it establishes bounds on effective properties of the composite. Semi-Empirical relationship has been suggested to related with the difficulties with the theoretical approaches described above. The micromechanics of load transfer and the correlation between constituent properties must be experimentally verified

4.3 MACROMECHNICS OF COMPOSITES

The stress and strain relations for a body can be given in indicial notation as

$$\sigma_{i_j} = \sum C_{ij} \times \varepsilon_j \left(i, j = 1,2,3...6\right)$$

where, C_{ij} = Material stiffness constants

For orthotropic material, the number of independent elastic constants are reduced to nine, as various stiffness and compliance terms are interrelated. The elastic constants include C_{ij} (i,j = 1,2,3), C_{44} , C_{55} , C_{66}. Here no coupling exists between normal stresses σ_1, σ_2, σ_3 and shear strains γ_4, γ_5, γ_6. No coupling prevails between shear stresses τ_4, τ_5, τ_6 & normal strains

ε_1, ε_2, ε_3. No coupling exists between shear stress acting on one plane and a shear strain on a different plane.

An orthotropic material is called a transversely isotropic when one of its principle planes is a plane of isotropy. The stress - strain relations are simplified by noting that subscripts 2 and 3 in the material constants are interchangeable. Here $C_{44} = (C_{22} - C_{23})/2$.

4.4 PLASTICITY IN COMPOSITES

Since the plasticity is modelled using micro-mechanical model, the plasticity of the individual constituents are modelled through conventional theories of plasticity. In order to model elasto-plastic materials' deformation, some conditions are to be fulfilled:

Just before the onset of plastic yield, the relationship between stress and strain is written by standard linear elastic expression.

$$\sigma_{ij} = C_{ijkl}\varepsilon_{kl} \tag{4.1}$$

The yield criterion may be given in general form

$$f(\sigma_{ij}) = K(k) \tag{4.2}$$

where, f and k are a function and a hardening parameter respectively.

Two most important yield criterions are Tresca Yield criterion and Von Mises Yield criterion.

Tresca criterion says that yielding begins at

$$\sigma_1 - \sigma_3 = Y(k) \tag{4.3}$$

where, $\sigma_1 \geq \sigma_2 \geq \sigma_3$ are the principal stresses and Y is a material parameter to be found experimentally and may be a function of hardening parameter k.

Von Mises yield criterion says that yielding occurs at J_2' reaches a critical value, or

$$\sqrt{J_2'} = K(k) \tag{4.4}$$

in which, K is a material parameter. The second deviatoric stress invariant J_2', can be written as

$$J_2' = \frac{1}{2}\left[\sigma_x'^2 + \sigma_y'^2 + \sigma_z'^2\right] + \tau_{xy}^2 + \tau_{yz}^2 + \tau_{zx}^2 \tag{4.5}$$

Yield criterion may be further written as

$$\bar{\sigma} = \sqrt{3J_2'} \tag{4.6}$$

where, $\bar{\sigma}$ is termed as effective stress, generalized stress or equivalent stress.

After starting yield the material behaviour will be partly elastic as well as plastic. During any increment of stress, the change of strain are considered to be divisible into elastic & plastic components, that is:

$$d\varepsilon_{ij} = (d\varepsilon_{ij})^e + (d\varepsilon_{ij})^p \tag{4.7}$$

The increment in elastic strain is related to the stress increment by Eq. (5.1). Decomposing the stresses into their deviatoric and hydrostatic components

$$(d\varepsilon_{ij})^e = \frac{d\sigma'_{ij}}{2\mu} + \frac{(1-2\nu)}{E}\delta_{ij} d\sigma_{kk} \tag{4.8}$$

where, E is an elastic modulus and ν is the Poisson's ratio.

To find the relationship between plastic strain components & stress increment, it can be assumed that the plastic strain increment is proportional to the stress gradient of a quantity known as plastic potential function Q, so that

$$(d\varepsilon_{ij})^p = d\lambda \frac{\partial Q}{\partial \sigma_{ij}} \tag{4.9}$$

where $d\lambda$ is a proportionality constant termed as the plastic multiplier.

CHAPTER 5

MODELLING OF INTERPENETRATING PHASE COMPOSITES

5.1 UNIT CELL MODEL

The smallest structural block that defines the structure of a composite with all information is called as a unit cell. It is also known as a representative volume element (RVE). The composite structure is made by putting numbers of unit cells. The micro-structural parameters such as volume fractions, distribution of phase and connectivity define a unit-cell.

5.1.1 Proposed Model

In **Figs 5.1-5.3**, the construction process of the unit cell is shown. A numbers of sub-cells combined together form the unit cell. Eight cuboids are placed at the each corner of a cube as shown in the **Fig.5.1**. The sum of the volumes that is, $V_1 + V_2 + \ldots + V_8$ of the cuboids bears a constant proportion to the volume (a^3) of the cube, where 'a' is the length of side of the cube. The ratio, thus obtained called the volume fraction (V_f) of the phase. When the cuboid's length is fixed the breadth and height needed to be calculated. The length of the cuboid is chosen randomly in a way that its value is smaller than half of the length of a sub-cell. After getting the length of the cuboid the breadth and height are evaluated.

$$V_f = \frac{V_1 + V_2 + V_3 + V_4 + V_5 + V_6 + V_7 + V_8}{a^3}$$

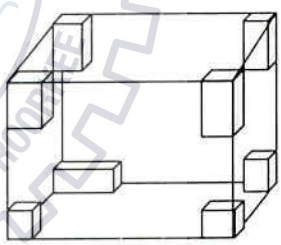

Figure 5.1a: Description of a single sub-cell (3D model)

$$V_f = \frac{A_1 + A_2 + A_3 + A_4}{a \times b}$$

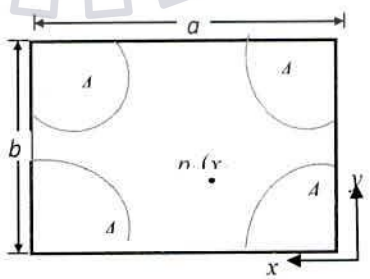

Figure 5.1b: Description of a single sub-cell (2D model)

Two types of sub-cell are developed to have interpenetrating nature, **Fig 5.2** shows both the sub-cells placed face by face. In type sub-cell the reinforcement is inside the cuboids and the remaining portion is filled with matrix phase, however the case is just reversed in type 2 sub-cells. When type 1 and type 2 sub-cells are used alternately, an interpenetrating structure of IPC is generated as shown in **Fig 5.3**. both the phases are interconnected and generated geometry is random in nature.

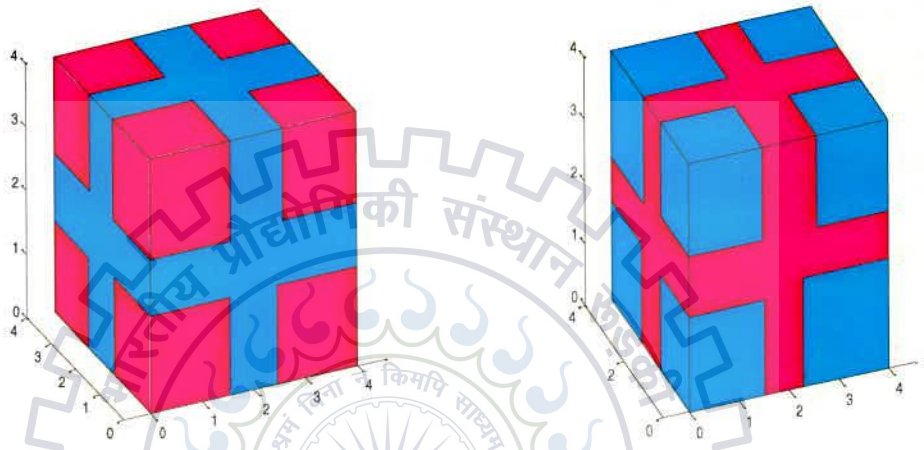

Figure 5.2: Different types of Sub-Cells (3D)

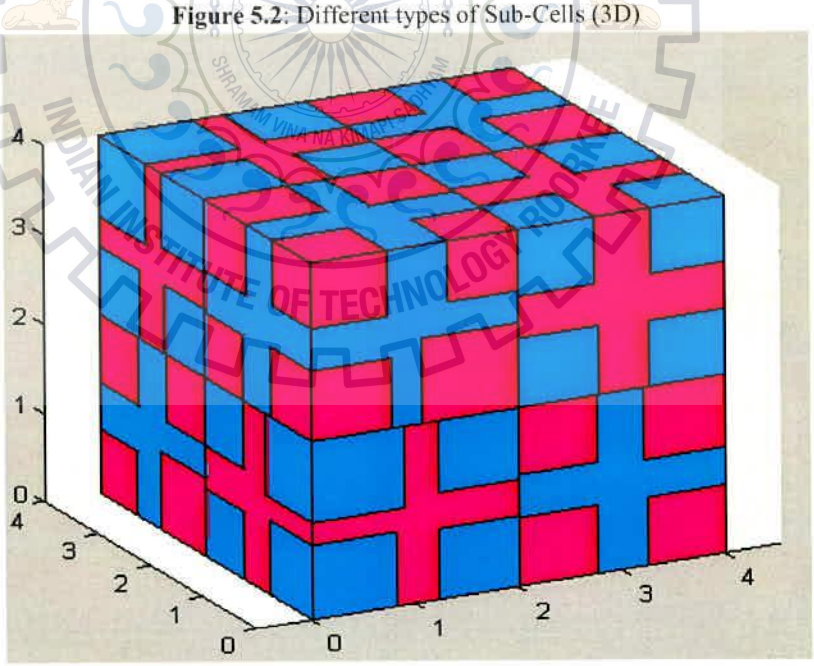

Figure 5.3: Proposed Unit Cell Model (3D)

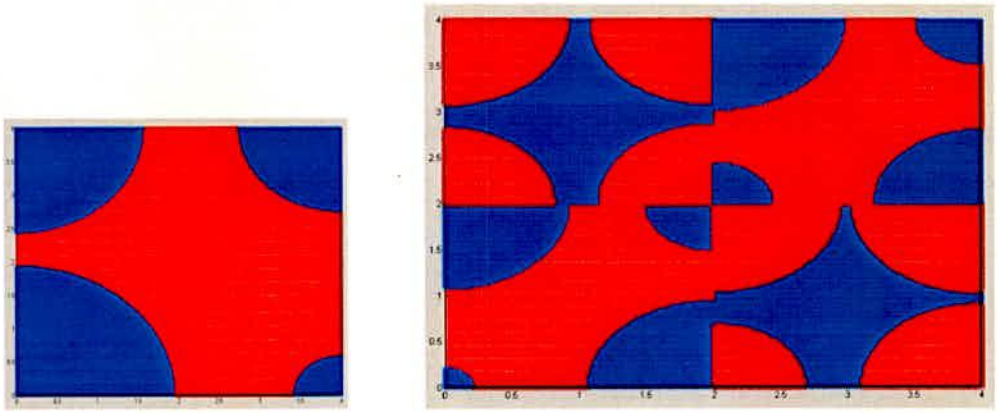

Figure 5.4 : Unit Cell Model (2D)

5.4.2 Implementation

The proposed unit-cell model is evaluated by Element Free Galerkin Method (EFGM). This model consists of cuboids, that don't need number of nodes to define its geometry in accurate sense, therefore the computational time reduced significantly. There are many techniques to model the interfaces. Howeveer, two different approaches, namely, domain partitioning technique & enrichment technique have been used in present work.

Enrichment technique has been used to model the interface. The normal distance from the interface of all the nodes is called signed distance. Since each cuboids has a three boundaries and hence, total 24 level set functions have been defined for each node. The split nodes are found near the boundary and respective level set function has been used. Three variables set are required for such level set function.

$$\phi_{i,j,k} = (x_{ijk} - x_{jki}, y_{jki} - y_{kij}, z_{kij} - z_{ijk},)$$

Where, i and j is the number of nodes in the domain and k is the number of cuboids representing a particular phase in a sub-cell (refer to **Fig 5.2**).

Besides the internal boundaries there are boundaries related to the interface of sub-cells. Domain portioning method has been used for those boundaries. The presence of other materials have been ignored to perform the integration. However, it is ensured that there must be some nodes on the boundaries.

In unit cell model the cub-cells are put together to form the model. Each nodes is assigned a property and data of each cellis reorganised to form a single structure. Thus, the implementation of a randomness becomes very easy and the domain partitioning method becomes simple to use.

Unidirectional constraints may not be used as an essential boundary conditions in a unit cell model. The periodic boundary conditions are relevant for the this model (Burla *et al.*, 2009 and Qingsheng *et al.*, 1994).

$u_L - u_R = Const$, $u_T - u_B = Const$ and $u_F - u_{BK} = Const$

where, L, R, T, B, F & BK stand for left, right, top ,bottom ,front and back face of the unit cell respectively.

The relevant boundary conditions for the two dimensional unit cell model to find Young's modulus and shear modulus are as shown in **Figures 5.4-5.5**.

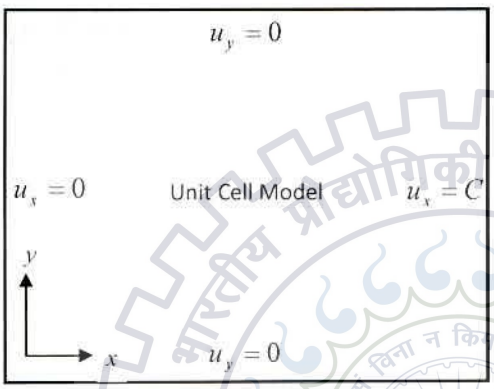

Figure 5.4: Periodic boundary condition to find Young's modulus (2D model)

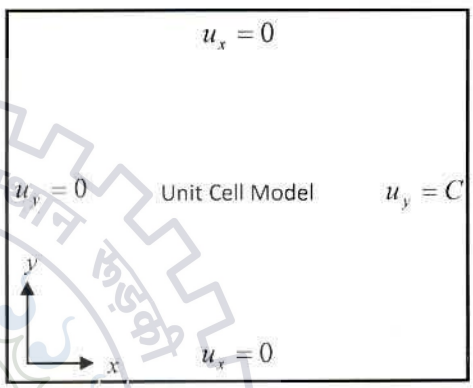

Figure 5.5: Periodic boundary condition to find Shear modulus (2D model)

5.4.3 Degree of Interpenetration

Both interpenetrating and dispersed phases are there in a real microstructure (Feng *et al.* 2003). The degree of interpenetration is a controlling parameter that affects the interpenetration of the phases. Based on the interpenetration three types of interpenetrations have been named such as high, low and medium. The particulate composite represents low interpenetration. A true IPC can be said to have high interpenetration. In medium interpenetration materials both interpenetrating and particulate phases exist.

Three types of composite behaviour can be found by just varying the geometry. The presence of eight cuboids at the corners of the cube is the unique feature of the model.

All eight cuboids lie at the eight corners of the cube for a high degree of interpenetration. In this way all reinforcement phase remain well connected the next sub-cell having reinforcement at the centre facilitate interpenetration.

All eight cuboids must be positioned at the centre of the cube for low interpenetration in type 1sub- cell and with no change in the type 2 sub-cell

some of the cuboids in Type-1 sub-cell are positioned to the centre, but others remain at the corners for the medium interpenetration.. Again, there will be no change geometry of type 2 sub- cell. This way medium degree of penetrations are found.

The proper implementation of the unit cell model has been demonstrated by the stress plots of the IPC as shown in **Fig 5.6 - 5.7**

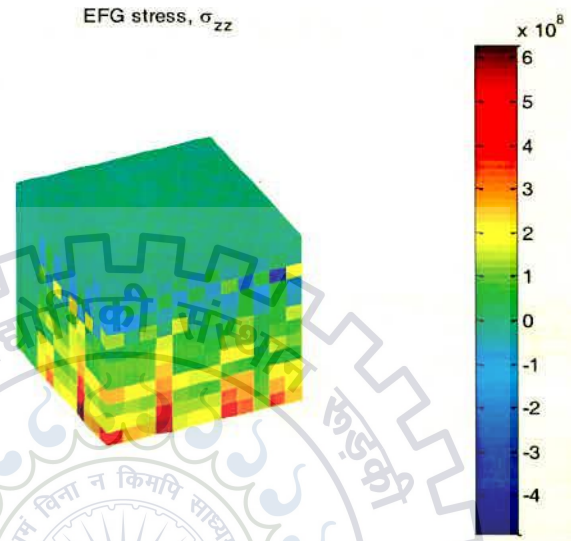

Figure 5.6: Shear stress plot of Unit cell model under shear stress

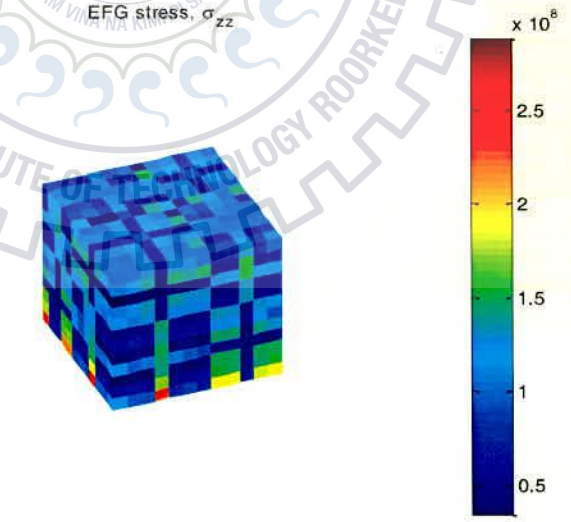

Figure 5.7: Normal stress plot for Unit cell model under Tensile loading

CHAPTER 6

EVALUATION OF ELASTIC PROPERTIES

6.1. EFFECTIVE MEDIUM APPROXIMATION

The composites are naturally homogeneous. Therefore, analysing the structure of composites is difficult task. To analyse composite structures we replace the heterogeneous composites by an equivalent homogeneous composites. This process is called an effective medium approximation. It comprises to find the mechanical properties of the equivalent homogeneous material. In modern time, researchers have used EMA approach to estimate the nature of cracks under thermo-mechanical loading for economical time. Reinforcement & matrix are interconnected throughout in IPC structure, this make EMA an effective tool to find out the equivalent mechanical properties of a composite.

Here, The principle of energy equivalence has been applied to evaluate mechanical properties of the equivalent material. Under the similar situation such as the load and boundary conditions the strain energy density for heterogeneous composites must be equal to equivalent homogeneous medium.

To evaluate the strain energy density a composite which is heterogeneous in nature numerical techniques approach has been used. However, in terms of unknown material properties the equivalent medium can be calculated analytically. In this thesis, Element Free Galerkin Method are used to evaluate strain energy density (as mentioned in section 3) of the composites which are heterogeneous in nature .

Therefore , the mechanical properties of the equivalent medium may be evaluated. The algorithm to evaluate effective properties of IPC is shown below.

(i) Recognise the domain computation from the physical geometry.

(ii) Recognise the relevant sets of boundary conditions based on the unknowns.

(iii) Numerically calculate strain energy density of the composite microstructure that is heterogeneous in nature with the use of following steps:

- To generate the microstructure composite model.
- Using EFGM analyse the microstructure.
- To calculate strain energy of using EFGM for particular domain.

(iv) To evaluate analytically the strain energy density of the equivalent medium which is homogeneous in nature as a function of unknown material.

(v) The strain energy of a medium which is homogeneous in nature be equated to the material properties of equivalent medium to evaluate an equation related it.

(vi) Go to the step (ii) for various sets of boundary conditions.

(vii) to find the equivalent properties of a medium a system of equation is calculated

As an example the whole calculation for an isotropic material is shown. Only two material properties such as, E and υ are required to completely define the stress strain relationship.

For two dimension problem

$$\begin{Bmatrix} \sigma_{xx} \\ \sigma_{yy} \\ \sigma_{xy} \end{Bmatrix} = \frac{E}{(1+\nu)(1-2\nu)} \begin{bmatrix} 1-\nu & \nu & 0 \\ \nu & 1-\nu & 0 \\ 0 & 0 & \frac{1-2\nu}{2} \end{bmatrix} \begin{Bmatrix} \varepsilon_{xx} \\ \varepsilon_{yy} \\ \gamma_{xy} \end{Bmatrix} \tag{6.1}$$

The strain energy U per unit volume of a body is given by

$$U = 0.5 \times (\sigma_{xx}.\varepsilon_{xx} + \sigma_{yy}.\varepsilon_{yy} + \sigma_{zz}.\varepsilon_{zz} + \sigma_{xy}.\gamma_{xy} + \sigma_{yz}.\gamma_{yz} + \sigma_{zx}.\gamma_{zx}) \tag{6.2}$$

To find the shear modulus (G), a uniform shear strain is applied in the whole body then Eq. (2) reduces to

$$U = 0.5 \times (\sigma_{xy}.\gamma_{xy}) \tag{6.3}$$

By substituting the values of σ_{xy} from Eq. (6.1) in Eq. (6.2), a relationship between the material property G ($G = E/(2 \times (1+\upsilon))$ and U is obtained as

$$U = 0.5 \times (G \times \gamma_{xy}^2) \tag{6.4}$$

The shear modulus G can be calculated in terms of total energy using Eq. (5.4) as:

$$G = 2 \times Energy/(\gamma_{xy}^2 \times L \times D) \tag{6.5}$$

The total energy is calculated numerically using EFGM.

To find Young' modulus (E), a uniform tensile strain is applied in one direction (say x-direction) then Eq. (5.2) reduces to

$$U = 0.5 \times (\sigma_{xx}.\varepsilon_{xx}) \tag{6.6}$$

By substituting the values of σ_{xx} from Eq. (5.1) in Eq. (5.6), a relationship between the material property E and total strain energy per unit thickness is obtained as

$$Energy = \frac{E \times (1-\upsilon) \times \varepsilon_{xx}^2 \times L \times D}{(1+\upsilon) \times (1-2\upsilon)} \tag{6.7}$$

$\upsilon = (E/2G) - 1$ is used in Eq. (5.7) to obtain the expression for E as

$$E = \frac{G \times (4G - 3C)}{G - C} \tag{6.8}$$

where, C is given by

$$C = \frac{2 \times Energy}{L \times D \times \varepsilon_{xx}^2}$$

Finally, the effective Poisson's ratio is calculated using the following relation

$$\upsilon = (E/2G) - 1 \tag{6.9}$$

For three dimension problem

$$U = 0.5 \times \frac{L \times D \times H}{G} \times P^2 \tag{6.10}$$

Where, L,D and H are length, breadth and height of the cube in metre (m) and P is load in Pa

$$G = \frac{L \times D \times H}{2U} \times P^2 \tag{6.11}$$

Using Numerical method the total energy U (Eq. 6.2) has been calculated and with shear load P (tau) = 100 MPa and the Eq.6.11, the shear modulus has been calculated. Thus, using the rest standard formulae Young's modulus has been calculated.

6.2 EFGM Algorithm

The algorithm for evaluating strain energy density of a composite material structure is nearly similar to the algorithm mentioned for the two – dimension problem,

After evaluating the values of stress and strains at each node, the strain energy density can be calculated by the integration of stresses and strains at each point.

$$U = \frac{1}{\overline{V}} \sum \int_{\Omega} \sigma_{ij} \cdot \varepsilon_{ij} \cdot d\overline{V} \tag{6.12}$$

CHAPTER 7

ELASTO-PLASTIC ANALYSIS OF IPC

7.1. ELASTO-PLASTIC SIMULATION

To simulate the elasto-plastic behaviour of IPC, accurate modelling of the microstructure is necessary. Different types of micro-mechanical models have been suggested in the literature. A unit cell model for the IPCs has already been proposed in chapter 5. A random microstructure model has also been proposed in chapter 5. The modelling and implementation of both the models has been explained. The elasto-plastic analysis has been done using EFGM in the chapter.

Both the constituent phases are modelled individually using the Ramberg-Osgood relation (Eq. 7.1).

$$\frac{\varepsilon}{\varepsilon_o} = \frac{\sigma}{\sigma_Y} + \alpha\left(\frac{\sigma}{\sigma_Y}\right)^n \tag{7.1}$$

This requires the use of two additional material constants (α , n) for each of the phases. α , n are the Ramberg-Osgood material constants/parameters. In the present work, the constants are calculated by curve fitting techniques so as to have the minimum error. The yield stress σ_Y is taken as the 2% proof stress. A line parallel to the elastic curve is drawn from 2% strain on x-axis. The point where the two curves meet denotes the yield stress of a material. The yield strain ε_o is the strain corresponding to the yield stress.

For numerical simulation, a load is given in small steps. In these load steps, the incremental stress is related to that of strain by effective moduli which depend on the present state of stress. A failure mechanism is introduced to simulate the effects of local material failure. The failure mechanism is same as that proposed by Yongqiang *et al.* (2007). A damage initiation criterion is used to all the nodes. As soon as the stress at any node reaches the ultimate strength corresponding to that node then it is treated as a failed node and a suitable correction in the material properties at that node is applied.

The failure of individual materials of the composite has been considered rather than the taking the failure criterion for the whole composite. The failure of each node inside the micro-mechanical model is governed by assumptions which are conventional in nature. In each load step, all the nodes are checked for failure using their individual stresses and

ultimate strength. Von-Mises failure criterion has been proposed for predicting local damage. If the Von-Mises stress at a particular node reaches the corresponding ultimate strength, then the stiffness of that node is reduced to a low value. In the next iteration, a analysis is performed again without increasing the load as some of the adjoining nodes might fail due to reduced stiffness of previously failed nodes. This is repeated until there is no further failure of nodes in a particular load step. Once the failure of any new node ceases, a new load step is applied in the usual manner. Thus, the composite is progressively damaged until no further stresses can be transferred.

The Von-Mises failure criterion is given by Eq. 2 and Eq. 3.

$$\sigma_v \geq \sigma_u \tag{7.2}$$

$$\sigma_v = \sqrt{\frac{1}{2}((\sigma_1 - \sigma_2)^2 + (\sigma_2 - \sigma_3)^2 + (\sigma_3 - \sigma_1)^2)} \tag{7.3}$$

where, σ_v is the Von-Mises stress and σ_i are the principal stresses in three mutually perpendicular directions. **Figure 7.1** shows the stress-strain curve for a material using Ramberg-Osgood model along with its failure mechanism. As soon as the stress reaches the ultimate strength (200 MPa in the present example), the stress becomes zero instantly at the node which results in the reduction of the overall stiffness of the composite due to the release of stress at the node. This relieved stress will be shared by the surrounding nodes thus increasing the stress in the surrounding region.

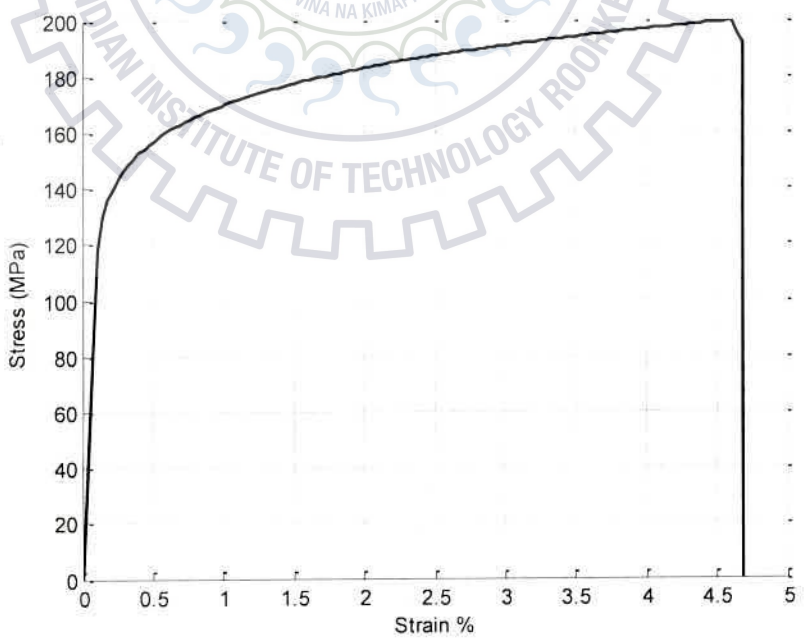

Figure 7.1: The stress-strain curve plot for a general node with damage

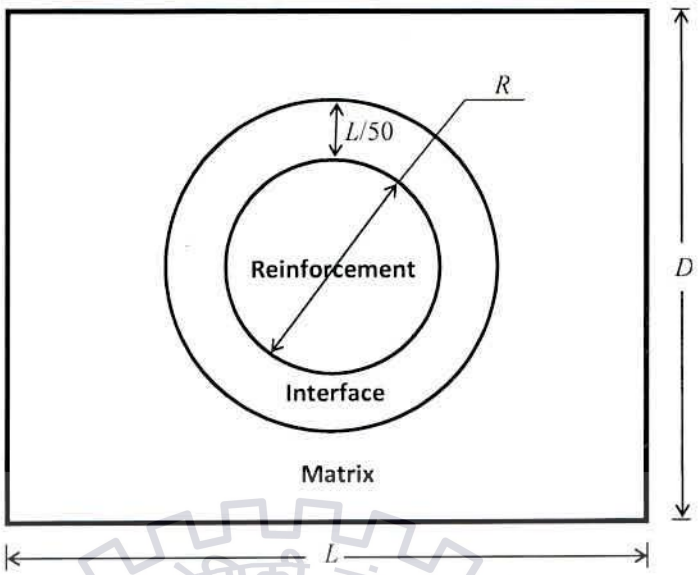

Figure 7.2: Interface representation in a particulate composite

The interface is defined as the transitional region between the matrix and the reinforcement (**Figure** 7.2). This region is important because the strength of the composite is largely affected by the type of bond between the two phases (Su *et al.*, 1999). A strong interface like a chemical bond enhances the strength of the composite. A weak interface may decrease the overall strength of the composite. Foo *et al.* (1993) studied the microscopic images of SiC interfaces. Pyo and Lee (2010) proposed a damage model considering the imperfect interface to predict the elasto-plastic behaviour of MMC. They used modified Eshelby tensor with weakened interfaces, and a progressive damage model to numerically simulate the multilevel interfacial damage model. The damage model has not been analysed because of the time constraints like getting the results in each run.

CHAPTER 8

RESULTS AND DISCUSSION

8.1 EFFECTIVE ELASTIC PROPERTIES

8.1.2 Unit Cell Model

In this work a composite material consisting of Alumina (Al_2O_3) and Copper (Cu) has been evaluated. The Young's moduli of Al_2O_3 and Cu are 390 GPa and 110 GPa , their shear moduli are 162 GPa and 40 GPa and Poisson's ratio are 0.20 and 0.34 respectively. Because, it is a random model, many runs have been taken to evaluate the statistical average. It is said that the results of all the runs are within 8% of the average values. Each data plotted is the statistical average of at least 5 runs of the same model for that particular data.

Fig 8.1 and Fig 8.2 show the convergence rate of a unit-cell model with respect to the total number of nodes in a sub-cell. In both the figures the convergence is at node 7 neglecting the abrupt change plot at 10 and 11^{th} node. Therefore, for all calculation purpose the no. of nodes taken is 7.

There has not been significant difference of the results for the selection of number of sub-cells. However, taking computational time into account the eight sub-cells has been considered for the evaluation purpose.

Figs 8.3-8.5 provide the effective shear modulus, Young's modulus and Poisson's ratio of the Interpenetrating Phase Composites w.r.t. the volume fraction of the Cu phase. It is observed that all the results fall within the theoretical bounds predicted by Voigt and Reuss. **Figures 8.3-8.5** are consistent with the experimental evidence that the material properties are largely dependent on volume fraction of a particular phase. **Figure 8.3** shows that the values of shear modulus predicted by the unit-cell model is higher than the values predicted by Poniznik *et al.*, 2008, the maximum difference being about 7%. It is on the higher side. It is approaching to the upper limit Similarly, **Figure 8.4** shows that the Young's modulii predicted by the unit-cell model is higher than the values predicted by Poniznik *et al.*, 2008, the maximum difference being 8%. It is again nearer to the upper limit. **Figure 8.5** shows that the values of Poisson's ratio predicted by the unit-cell model is higher than the values predicted by Poniznik *et al.*, 2008. The Poisson's ratio has been calculated from the formula $\upsilon = (E/2G) - 1$ where the E and G are the predicted values.

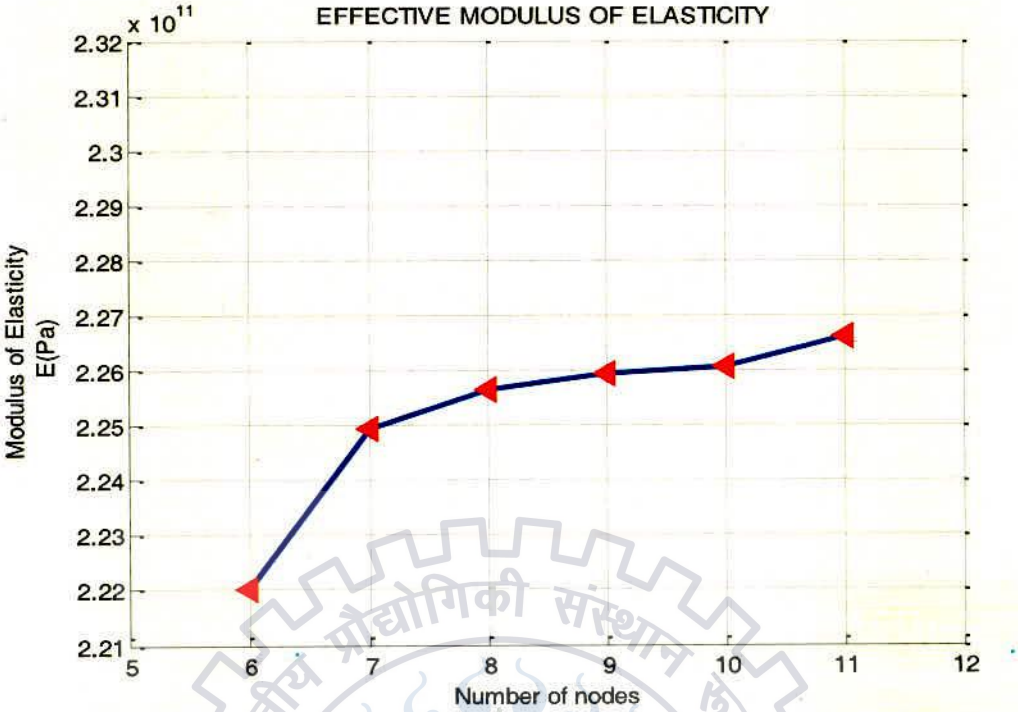

Figure 8.1: Convergence of unit cell model with respect to total number of nodes

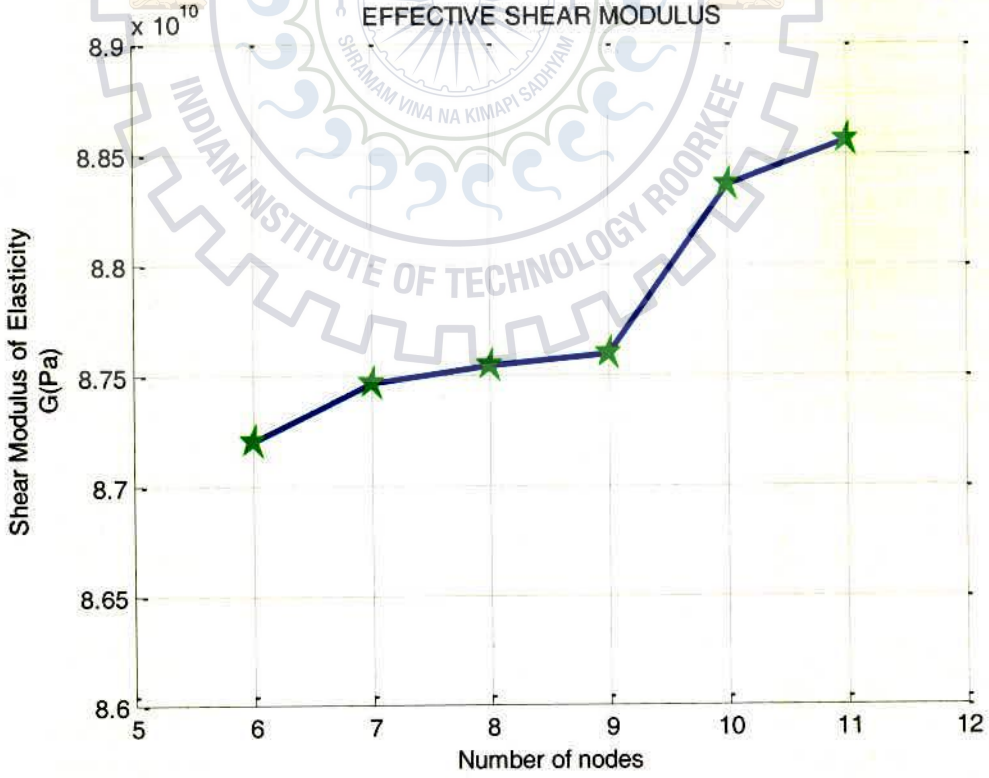

Figure 8.2: Convergence of unit cell model with respect to total number of sub-cells

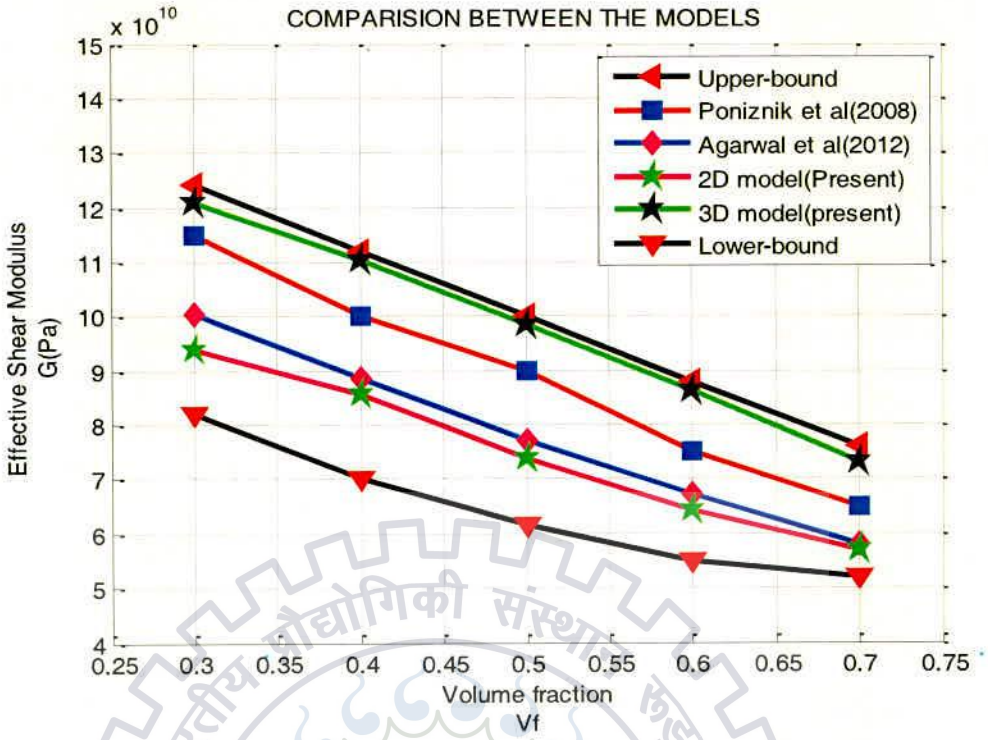

Figure 8.3: Variation of shear modulus with volume fraction of Cu phase

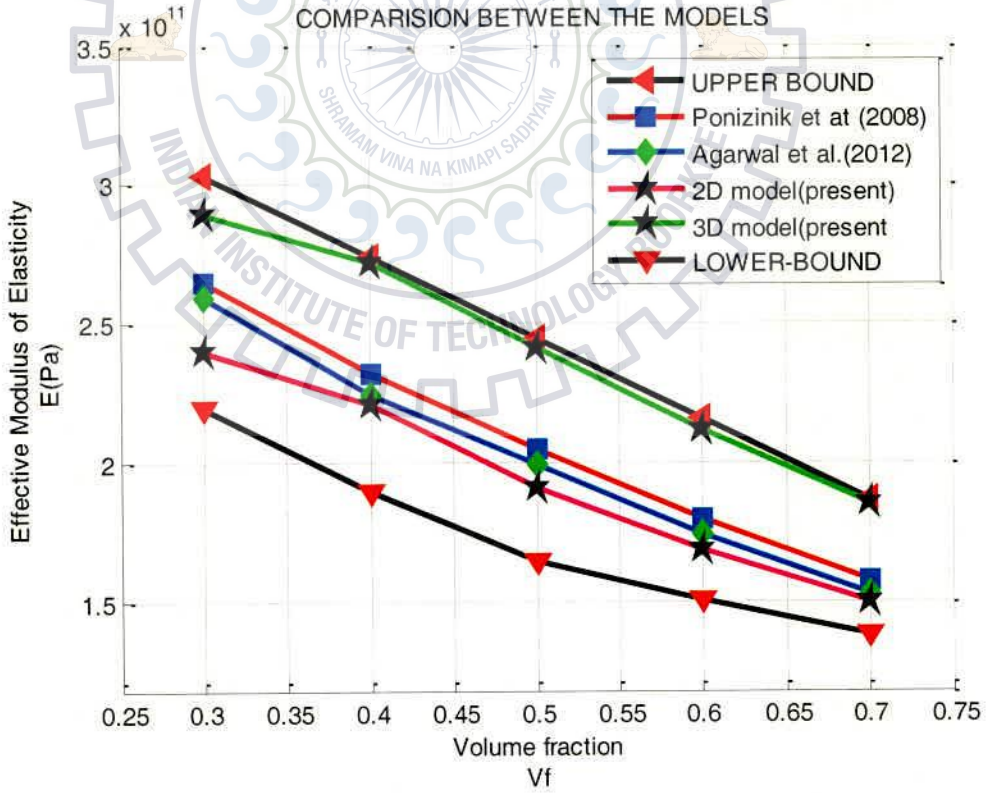

Figure 8.4: Variation of Young's modulus with volume fraction of Cu phase

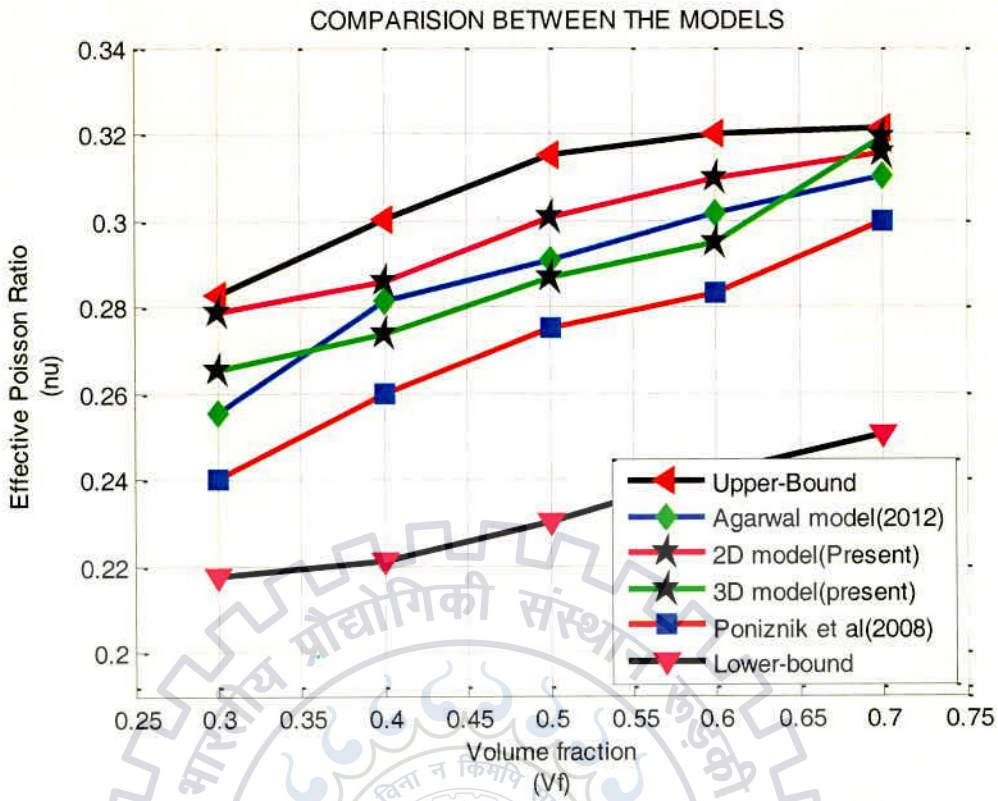

Figure 8.5: Variation of Poisson's ratio with volume fraction of Cu phase

Finally, the results of the proposed unit-cell model are compared with the experimental results obtained by Poniznik *et al,* 2008, in **Figs 8.3-8.5**. It can be seen that the experimental values lie between the predictions of the proposed unit-cell model in 2-D and 3-D model given by Poniznik *et al,* 2008. Moreover, the difference between the prediction of the proposed unit-cell model and the 3-D model of Poniznik is less than 8%. The proposed unit cell model(2D) is easier to implement and computationally less expensive. However, taking readings for the three dimensional problems was tedious job as it was time intensiveness process.

CHAPTER 9

CONCLUSION AND FUTURE SCOPE

In the present thesis, two models of IPCs have been proposed one in two dimension and another in three dimension. All dominating parameters like volume fraction & random geometry that may affect the properties of IPCs are considered in modelling to obtain an accurate simulation. The model has been made preferably using EFGM than FEM taking advantages of element free modelling. The effective medium enrichment technique has been used to model the interface between two materials. Parameters controlling the degree of penetration have been incorporated into the model. This way the composites can be modelled with partial or no interpenetration to predict effectively the elastic properties of the materials

The proposed unit cell model (2D) is easier to implement and less expensive as far as computation is concerned in comparison to earlier models. However, the 3D model emulates the actual composite and said to be giving proper mechanical properties but time intensive. Using basic geometry and probability the random microstructure model is generated. The effective mechanical properties of IPC can be predicted by the models for combination of materials and volume fractions (0.3 to 0.7).

The future scope of the work is as follows

- The fracture mechanics concepts may be used to simulate crack propagation in IPCs.
- The thermal analysis, crack propagation, interface analysis may be explored.
- The analysis of void nucleation and damage propagation needs to be explored in detail.
- The parameters like dislocation density, crack bridging mechanisms, random distribution of phases, etc have to be incorporated into the model as they greatly affect the mechanical behaviour of these composites.
- The structural analysis using the microstructure of IPC can be performed.
- The effect of imperfect interface can be modelled in IPC.

भारतीय प्रौद्योगिकी संस्थान रुड़की
श्रमं विना न किमपि साध्यम्
SHRAMAM VINA NA KIMAPI SADHYAM
INDIAN INSTITUTE OF TECHNOLOGY ROORKEE

REFERENCES

Agarwal A., Singh, I.V., Mishra B.K., Numerical prediction of elasto-plastic behaviour of interpenetrating phase composites by EFGM, *Composites*; Part B 51 page 327-336, 2013

Agarwal A., Singh I.V., Mishra B.K., Evaluation of elastic properties of interpenetrating phase composites by mesh-free method., *Journal of Composite Materials*.,0(0)p1-17,2012

Agrawal P, Sun C.T., Fracture in metal–ceramic composites, *Composites Science and Technology*, Vol. 64, pp. 1167–1178, 2004.

Agrawal P., Conlon K., Bowman K.J., Sun C.T., JR Cichocki F.R., Trumble K.P., Thermal residual stresses in co-continuous composites, *Acta Materialia*, Vol. 51, pp. 1143–1156, 2003.

Basista M and Węglewski W, Modelling of Damage and Fracture in Ceramic Matrix Composites–An Overview, *Journal of Theoretical and Applied Mechanics*, Vol. 44, pp. 455–484, 2006.

Belytschko T., Fleming M., Smoothing, enrichment and contact in element free Galerkin method, *Computers and Structures*, Vol. 71, pp. 173–195, 1999.

Belytschko T., Krongauz Y., Fleming M., Organ D.J. and Liu W.K. Smoothing and accelerated computations in the element free Galerkin method, *Journal of Computational and Applied Mathematics*; Vol. 74, pp. 111–126, 1996.

Belytschko T., Kroungauz Y., Organ D., Fleming M., Krysl P., Meshless methods: an overview and recent developments, *Computer Methods in Applied Mechanics in Engineering*, Vol. 139, pp. 3–47, 1996.

Belytschko T., Lu Y.Y., Gu L., Crack propagation by element free Galerkin methods, *Engineering Fracture Mechanics*, Vol. 51, pp. 295–315, 1995a.

Belytschko T., Lu Y.Y., Gu L., Element-free Galerkin methods, *International Journal for Numerical Methods in Engineering*, Vol. 37, pp. 229–256, 1994.

Belytschko T., Lu Y.Y., Gu L., Numerical solutions of mixed mode dynamic fracture in concrete using element free Galerkin methods, *ICES Conference Proceedings*, 1995b.

Belytschko T., Organ D., Krongauz Y., A coupled finite element- element free Galerkin method, *Computational Mechanics*, Vol. 17, pp. 186–195, 1996a.

Belytschko T., Organ D., Krongauz Y., Fleming M., Smoothing and accelerated computations in element free Galerkin methods, *Journal of Computational and Applied Mathematics*, Vol. 74, pp. 111–126, 1996b.

Bin S, Wen-bin H., Lei L., Wei Z., Di Z., Metal-matrix interpenetrating phase composites produced by squeeze casting, *Transactions of Nonferrous Metals Society of China*, Vol. 12, pp. 26-29, 2002.

Burla R.K., Kumar A.V., Sankar B.V., Implicit boundary method for determination of effective properties of composite microstructures, *International Journal of Solids and Structures*, Vol. 46, pp. 2514–2526, 2009.

Chessa J, Smolinski P, Belytschko T. The extended finite element method (XFEM) for solidi_cation problems. *International Journal for Numerical Methods in Engineering*; Vol. 53, pp. 1959–1977, 2002.

Chinh N.Q., Horvath G., Horita Z., Langdon T. G., A new constitutive relationship for the homogeneous deformation of metals over a wide range of strain, *Acta Materialia*, Vol. 52, pp. 3555–3563, 2004.

Doe T. J. A., Bowen P., Tensile properties of particulate-reinforced metal matrix composites, *Composites Part A*, Vol. 27A, pp. 655-665, 1995.

Dolbow J., Belytschko T., Numerical integration of Galerkin weak form in meshfree methods, *Computational Mechanics,* Vol. 23, pp. 219–230, 1999.

Dukhan N., Rayess N., Hadley J., Characterization of aluminum foam–polypropylene interpenetrating phase composites: Flexural test results, *Mechanics of Materials*, Vol. 42, pp. 134–141, 2010.

Etter T., Kuebler J., Frey T., Schulz P., Loffler J.F., Uggowitzer P.J., Strength and fracture toughness of interpenetrating graphite/aluminium composites produced by the indirect squeeze casting process, *Materials Science and Engineering*: A, Vol. 386, pp. 61–67, 2004.

Feng X.Q., Tian Z., Liu Y, Yu S, Effective elastic and plastic properties of interpenetrating multiphase composites, *Applied Composite Materials,* Vol. 11, pp. 33–55, 2004.

Feng Xi-Qiao, Mai Yiu-Wing, Qin Qing-Hua, A micromechanical model for interpenetrating multiphase composites, *Computational Materials Science*, Vol. 28, pp. 486–493, 2003.

Fleming W.J., Temis J.M., Numerical simulation of cyclic plasticity and damage of an aluminium metal matrix composite with particulate SiC inclusions, *International Journal of Fatigue,* Vol. 24, pp. 1079–1088, 2002.

Foo K.S., Banks W.M., Craven A.J., Hendry A. Interface characterization of an SiC particulate/6061 aluminium alloy composite, *Composites,* Vol. 25, No. 7, pp. 677-683, 1993.

Gonziilez C., Llorca J., Prediction of the tensile stress-strain curve and ductility in Al/SiC composites, *Scripta Materialia*, Vol. 35, No. 1, pp. 91–97, 1996

Gravouil A, Moes N, Belytschko T. Non-planar 3D crack growth by the extended finite element and level sets part II: Level set update, *International Journal for Numerical Methods in Engineering*; Vol. 53, pp. 2659–2586, 2002.

Hertele S., Waele W. D., Denys R., A generic stress–strain model for metallic materials with two-stage strain hardening behaviour, *International Journal of Non-Linear Mechanics* , Vol. 46, pp. 519–531, 2011.

Horvitz D., Gotman I., Gutmanas E.Y., Claussen N., In situ processing of dense Al2O3–Ti aluminide interpenetrating phase composites, *Journal of the European Ceramic Society*, Vol. 22, pp. 947–954, 2002.

Hsu T.R., The finite element method in thermodynamics, *Allen and Unwin Inc.,* London, U.K., 1986.

Jhaver R. and Tippur H., Processing, Compression response and finite element modeling of syntactic foam based interpenetrating phase composite (IPC), *Materials Science and Engineering: A*, Vol. 499, pp. 507–517, 2009.

Kaminski M. and Kleiber M., Numerical homogenization of N-component composites including stochastic interface defects, *International Journal for Numerical Methods in Engineering*, Vol. 47, pp. 1001–1027, 2000.

Kapoor, R., Vecchio K.S., Deformation behavior and failure mechanisms in particulate reinforced 6061 Al metal-matrix composites, *Materials Science and Engineering A*, Vol. 202, pp. 63-75, 1995.

Kashyap K.T., Ramachandra C., Dutta C., Chatterji B., Role of work hardening characteristics of matrix alloys in the strengthening of metal matrix composites, *Bulletin of Material Science*, Vol. 23, No. 1, pp. 47–49. 2000.

Kouzeli M., Dunand D.C., Effect of reinforcement connectivity on the elasto-plastic behavior of aluminum composites containing sub-micron alumina particles, *Acta Materialia*, Vol. 51, pp. 6105–6121, 2003.

Krangauz Y., Belytschko T., Enforcement of essential boundary conditions in meshless approximations using finite elements, *Computer Methods in Applied Mechanics and Engineering,* Vol.131, pp. 133–145, 1996.

Krongauz Y. and Belytschko T., EFG approximation with discontinuous derivative, *International Journal for Numerical Methods in Engineering*, Vol. 41, pp. 1215-1233, 1998.

Lapczyk I., Hurtado J A., Progressive damage modeling in fiber-reinforced materials, *Composites: Part A*, Vol. 38, pp. 2333–2341, 2007.

Liu W., Koster U., Microstructures and properties of interpenetrating alumina/aluminium composites made by reaction of SiO2 glass preforms with molten aluminium, *Materials Science and Engineering: A*, Vol. 210, pp. 1-7, 1996.

Liu Y, Gong X., Compressive behavior and energy absorption of metal porous polymer composite with interpenetrating network structure, *Transactions of Nonferrous Metals Society of China*, Vol. 16, pp. 439–443, 2006.

Lu Y. Y, Belytschko T., Gu L. and Tabbara M, Element free Galerkin method for wave propagation and dynamic fracture, *Computer Methods in Applied Mechanics and Engineering*, Vol. 126, pp. 131-153, 1995

Lu Y. Y, Belytschko T., Gu L., Tabbara M., A new implementation of element free Galerkin method, *Computer Methods in Applied Mechanics and Engineering*, Vol. 113, pp. 397–414, 1994.

Marchi C. San, Kouzeli M., Rao R., Lewis J.A., Dunand D.C., Alumina–aluminum interpenetrating-phase composites with three-dimensional periodic architecture, *Scripta Materialia*, Vol. 49 , pp. 861–866, 2003.

Mayer H., Papakyriacou M., Fatigue behaviour of graphite and interpenetrating graphite–aluminium composite up to 109 load cycles, *Carbon*, Vol. 44, pp. 1801–1807, 2006.

Moes N, Dolbow J, Belytschko T., A finite element method for crack growth without remeshing, *International Journal for Numerical Methods in Engineering*; Vol. 46, pp. 31-150, 1999.

Moon R. J., Hoffman M., Rödel J., Tochino S., Pezzotti G., Evaluation of crack-tip stress fields on microstructural-scale fracture in Al–Al2O3 interpenetrating network composites, *Acta Materialia*, Vol. 57, pp. 570–581, 2009.

Periasamy C., Tippur H.V., Experimental measurements and numerical modelling of dynamic compression of interpenetrating phase composite foam, Mechanics Research Communications., 43 page 57-65, 2012

Periasamy C., Jhaver R., Tippur H.V., Quasi-static and dynamic compression response of a lightweight interpenetrating phase composite foam, *Materials Science and Engineering: A*, Vol. 527, pp. 2845–2856, 2010.

Pezzotti G., Sbaizero O., Residual and bridging microstress fields in Al_2O_3/Al interpenetrating network composite evaluated by fluorescence spectroscopy, *Materials Science and Engineering A*, Vol. 303, pp. 267–272, 2001.

Poniznik Z., Salit V., Basista M., Gross D., Effective elastic properties of interpenetrating phase composites, *Computational Materials Science*, Vol. 44, pp. 813–820, 2008.

Prielipp H., Knechtel M., Claussen N., Streiffer S. K., Mulejans H., Ruhle M., Rodel J., Strength and fracture toughness of aluminum/alumina composites with interpenetrating networks, *Materials Science and Engineering* A, Vol. 197, pp.19-30, 1995.

Pyo S.H., Lee H.K., An elastoplastic damage model for metal matrix composites considering progressive imperfect interface under transverse loading, *International Journal of Plasticity*, Vol. 26, pp. 25–41, 2010.

Qingsheng Y., Limin T., Haoran C., Self-consistent finite element method: A new method of predicting effective properties of inclusion media, *Finite Elements in Analysis and Design*, Vol. 17, pp. 247–257, 1994.

Quang H.L., He Q.C., A one-parameter generalized self-consistent model for isotropic multiphase composites, *International Journal of Solids and Structures*, Vol. 44, pp. 6805–6825, 2007.

Rao B.N. and Rahman S., An efficient meshless method for fracture analysis of cracks, Computational Mechanics, Vol. 26, pp. 398–408, 2000.

Ravichandran K.S., Deformation behaviour of interpenetrating phase composites, *Composites Science and Technology,* Vol. 52, pp. 541–549, 1994.

Reddy A.C., Zitoun E., Matrix Al-alloys for silicon carbide particle reinforced metal matrix composites, *Indian Journal of Science and Technology,* Vol. 3, pp. 12, 2010.

Rossoll A., Moser B., Mortensen A., Tensile strength of axially loaded unidirectional Nextel 610™ reinforced aluminium: A case study in local load sharing between randomly distributed fibres, *Composites: Part A*, Vol. 43, pp. 129–137, 2012

Scherm F., Völkl R., Neubrand A., Bosbach F., Glatzel U., Mechanical characterisation of interpenetrating network metal–ceramic composites, *Materials Science and Engineering A*, Vol. 527, pp. 1260–1265, 2010.

Shen W., Tang C.Y., Tsui C.P., Peng L.H., Effects of two damage mechanisms on effective elastic properties of particulate composites, *Composites Science and Technology,* Vol. 62, pp. 1397–1406, 2002.

Sosa J. L. C., Petrinic N., Wiegand J., A three-dimensional progressive damage model for fibre-composite materials, *Mechanics Research Communications*, Vol. 35, pp. 219–221, 2008.

Su X.F., Chen H.R., Kennedy D., Williams F.W., Effects of interphase strength on the damage modes and mechanical behaviour of metal–matrix composites, *Composites: Part A*, Vol. 30, pp. 257–266, 1999.

Teoh S.H., Sivaramakrishnan M. R., Thampuran R., Tensile and fracture properties of titanium-polymer interpenetrating network composites, *Journal of Materials Science Letters,* Vol. 15, pp. 1478–1480, 1996.

Tilbrook M.T., Moon R.J., Hoffman M., On the mechanical properties of alumina–epoxy composites with an interpenetrating network structure, *Materials Science and Engineering A*, Vol. 393, pp. 170–178, 2005.

Tohgo K., Masunari A., Yoshida M., Two-phase composite model taking into account the matricity of microstructure and its application to functionally graded materials, *Composites: Part A*, Vol. 37, pp. 1688–1695, 2006.

Torquato S., Modeling of physical properties of composite materials, *International Journal of Solids and Structures*, Vol. 37, pp. 411–422, 2000.

Vecchia G. M. L., Badini C., Puppo D., D'errico F., Co-continuous Al/Al2O3 composite produced by liquid displacement reaction: Relationship between microstructure and mechanical behavior, *Journal of Materials Science*, Vol. 38, pp. 3567–3577, 2003.

Wang M, Pan N, Elastic property of multiphase composites with random microstructures, *Journal of Computational Physics*, Vol. 228, pp. 5978–5988, 2009.

Wegner L.D, Gibson L.J, The fracture toughness behaviour of interpenetrating phase composites, *International Journal of Mechanical Sciences*, Vol. 43, pp. 1771–1791, 2001b.

Wegner L.D., Gibson L.J., The mechanical behaviour of interpenetrating phase composites - II: a case study of a three-dimensionally printed material, *International Journal of Mechanical Sciences*, Vol. 42, pp. 943–964, 2000.

Wegner L.D., Gibson L.J., The mechanical behaviour of interpenetrating phase composites-III: resin-impregnated porous stainless steel, *International Journal of Mechanical Sciences*, Vol. 43, pp. 1061–1072, 2001a.

Xu X.F., Graham Brady L., A stochastic computational method for evaluation of global and local behavior of random elastic media, *Computational Methods Applied Mechanical Enggineering*, Vol. 194, pp. 4362–4385, 2005.

Yongqiang C., Shuli S., Yi L., Numerical Simulation of the Mechanical Properties and Failure of Heterogeneous Elasto-Plastic Materials, *Tsinghua Science and Technology*, ISSN 1007-0214 04/19, Vol. 12, Number 5, pp. 527–532, 2007.

Zen Ching Han, Brown Ian W.M., Zhang D.L., Microstructure development and properties of alumina–Ti aluminide interpenetrating composites, *Current Applied Physics*, Vol. 6, pp. 444–447, 2006.

Zhou W., Hu W., Zhang D., Metal-matrix interpenetrating phase composite and its in situ fracture observation, *Materials Letters*, Vol. 40, pp. 156–160, 1999.

Zhou W., Hu W., Zhang D., Study on the making of metal-matrix interpenetrating phase composites, *Scripta Materialia*, Vol. 39, pp. 1743–1748, 1998.

Zhou Y., Huang W., Xia Y., A microscopic dynamic Monte Carlo simulation for unidirectional fiber reinforced metal matrix composites, *Composites Science and Technology*, Vol. 62, pp. 1935–1946, 2002